

Communications Research Centre

MEASUREMENTS OF VHF/UHF RADIO PROPAGATION IN A MARITIME TEMPERATE CLIMATE

by

J.H. Whitteker

CRC REPORT NO. 1380

OTTAWA, MARCH 1985

Canada

TK
5102.5
C673e
#1380



Canada
Communications

Gouvernement du Canada
Ministère des Communications

COMMUNICATIONS RESEARCH CENTRE

DEPARTMENT OF COMMUNICATIONS
CANADA

**MEASUREMENTS OF VHF/UHF RADIO PROPAGATION
IN A MARITIME TEMPERATE CLIMATE**

by
J.H. Whitteker

(Radar and Communications Technology Branch)

Industry Canada
Library - Queen

AOUT 27 2012
AUG

Industrie Canada
Bibliothèque - Queen



CRC REPORT NO. 1380

March 1985

OTTAWA

CAUTION

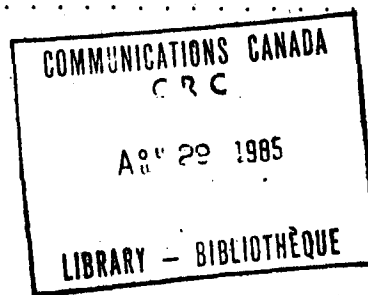
This information is furnished with the express understanding that:
Proprietary and patent rights will be protected.

TK
5102.5
C673e
#1380
C. b

2A 5533742
2L 5533766

TABLE OF CONTENTS

ABSTRACT	1
1. INTRODUCTION	1
1.1 Motivation and Related Work	1
1.2 Site Selection	1
1.3 Propagation Paths	3
2. EQUIPMENT FOR RECEIVING AND RECORDING	4
2.1 Receiving Equipment	4
2.2 Data Recording	5
2.3 Calibration	5
3. DATA ANALYSIS	6
3.1 Path Loss	6
3.2 Effective Radiated Power	6
3.3 Hourly Distributions	6
3.4 Diurnal Variation	7
3.5 Distribution for All Hours of the Day	7
4. LONG-TERM MEDIAN PATH LOSS	7
4.1 Measured Path Loss	7
4.2 Predicted Median Path Loss	8
5. VARIATION OF SIGNAL — TIME SERIES	9
5.1 Time Series of Hourly Medians	9
5.2 Autocorrelation of Time Series	9
5.3 One-Year Plots of Daily Medians	9
6. CUMULATIVE DISTRIBUTIONS OF RECEIVED POWER	22
6.1 Distribution Plots	22
6.2 Comparison with Other Measurements	23
7. ANNUAL VARIATION	27
7.1 Observations	27
7.2 Model of Results	27
7.2.1 Time Factor	27
7.2.2 Distance Factor — Overland and Mixed Paths	28
7.2.3 Model of Annual Variation — Overland and Mixed Paths	29
7.2.4 Model of Annual Variation — Oversea Paths	29
7.2.5 Other Measurements	29



8. DIURNAL VARIATION	29
8.1 Observations	29
8.1.1 Plots of Diurnal Variation	29
8.1.2 Numerical Summary of Diurnal Variation	33
8.2 Model of Diurnal Variation	34
8.2.1 Time Factor — Overland and Mixed Paths	34
8.2.2 Distance Factor — Overland and Mixed Paths	34
8.2.3 Model of Diurnal Variation — Overland and Mixed Paths	34
8.2.4 Model of Diurnal Variation — Oversea Paths	35
8.2.5 Other Measurements	35
9. CONCLUSIONS	36
10. ACKNOWLEDGEMENTS	36
11. REFERENCES	37
APPENDIX A - Mean Carrier Amplitude	38
APPENDIX B - Post-mortem Measurements of Field Strength	40

MEASUREMENTS OF VHF/UHF RADIO PROPAGATION IN A MARITIME TEMPERATE CLIMATE

by

J.H. Whitteker

ABSTRACT

The signal strength from five television transmitters was monitored for two years at a site near Yarmouth, Nova Scotia. The path lengths ranged from 92 to 384 km, and the frequencies from 67 to 543 MHz. Two of the paths were overland, one path (with two transmitters) was mixed, and one path was over sea. The long-term median signal levels can be approximated by standard path-loss predictions if foliage attenuation is taken into account. The long-term statistical distribution of signal levels is in accord with the curves of NBS Technical Note 101, except that oversea UHF received power levels exceeded 10% of the time were found to be 10 to 20 dB higher than in the curves. The range of the seasonal variation of the monthly median signal level was found to be from 5 to 16 dB, with the greatest variation on the long oversea path. The range of the diurnal variation of the hourly median signal was found to be from zero to 7 dB, with the greatest variation in the summer and the most prominent variation on the shortest path. Signals were strongest in summer and in early morning.

1. INTRODUCTION

1.1 MOTIVATION AND RELATED WORK

The signal strength received over a path longer than about 50 km varies with time because of changes in the refractive index of the atmosphere. The statistics of these variations are known in a general way for several global climatic types (1-6). However, predictions for a particular region can be made with confidence only if measurements have been made in that region. An earlier CRC Report (7) describes measurements made in the Great Lakes region of North America. The present report gives results obtained during two years of monitoring several television signals at a site near Yarmouth, Nova Scotia. The data were provided by Technical University of Nova Scotia, and its report (8) describes the data collection and gives preliminary results, including reproductions of selected chart records.

Other measurements have recently been made in the Atlantic provinces. A report by St. Mary's University (9) gives results for paths from Sable Island to mainland Nova Scotia. Measurements across Trinity Bay in Newfoundland were done by Memorial University, but as of the time of writing, no results have been published. The work done by all three universities was performed under contract to the Department of Communications.

1.2 SITE SELECTION

A monitoring site was established at a microwave relay station near the village of Hebron, 7 km NE of Yarmouth, Nova Scotia. The site was chosen by representatives of both CRC and Technical University of Nova Scotia, who made test measurements at candidate sites. The Hebron site proved to be one from which several distant television transmitters could be monitored without co-channel interference. The microwave relay station is operated by the Maritime Telegraph and Telephone Company (MT&T). The receiving antennas were mounted on the microwave tower, and an MT&T technician took care of the recording equipment.

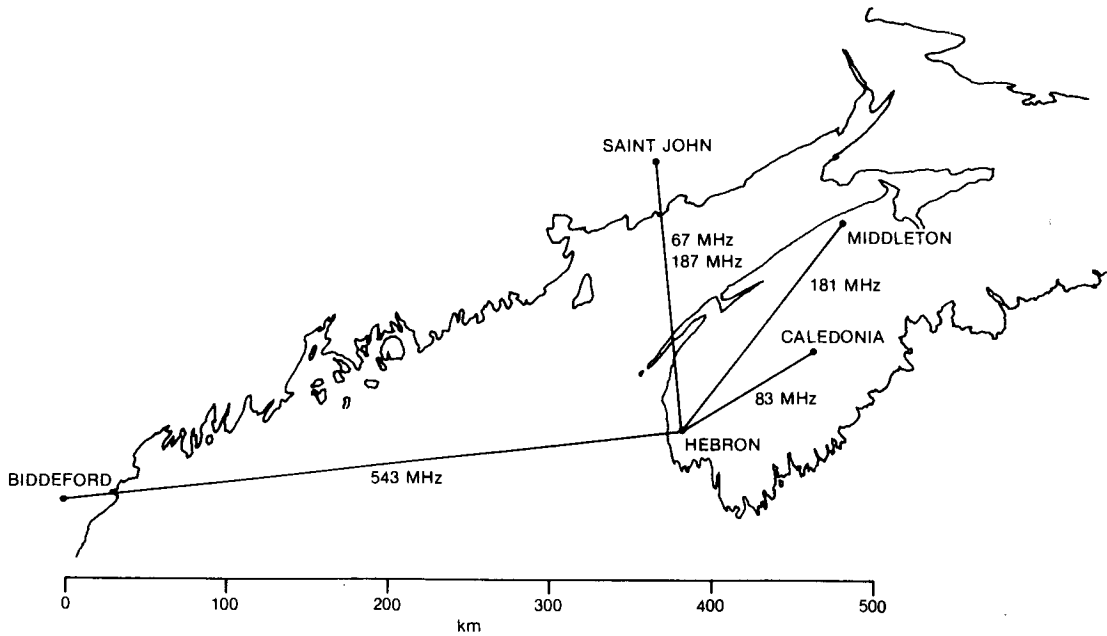


Figure 1. The locations of the receiving site (Hebron) and of the television transmitters.

TABLE 1
Station Coordinates

Station	Location		Azimuth		Antenna Height
			Rx→Tx	Tx→Rx	
Caledonia	44° 20' 26" N	65° 6' 34" W	57°	238°	295 m
Middleton	45° 4' 38" N	64° 49' 2" W	37°	218°	323 m
Saint John 4	45° 28' 39" N	66° 14' 2" W	356°	176°	487 m
Saint John 9	45° 28' 39" N	66° 14' 2" W	356°	176°	517 m
Biddeford	43° 25' 0" N	70° 48' 9" W	264°	80°	368 m
Hebron	43° 53' 46" N	66° 4' 34" W			57, 60 m (above sea level)

TABLE 2
Transmission Paths

Tx Name	Path Length	Effective		TV Channel	Carrier Frequency
		Distance	Surface		
Caledonia	92 km	91 km	land	6 ⁺	83.260 MHz
Middleton	165 km	186 km	land	8 ⁻	181.240 MHz
Saint John 4	176 km	121 km	mixed	4 ⁺	67.260 MHz
Saint John 9	176 km	137 km	mixed	9 ⁺	187.260 MHz
Biddeford	384 km	366 km	sea	26 ⁻	543.240 MHz

Note: Under 'TV Channel', the + or - indicates the sign of a 10 kHz frequency offset.

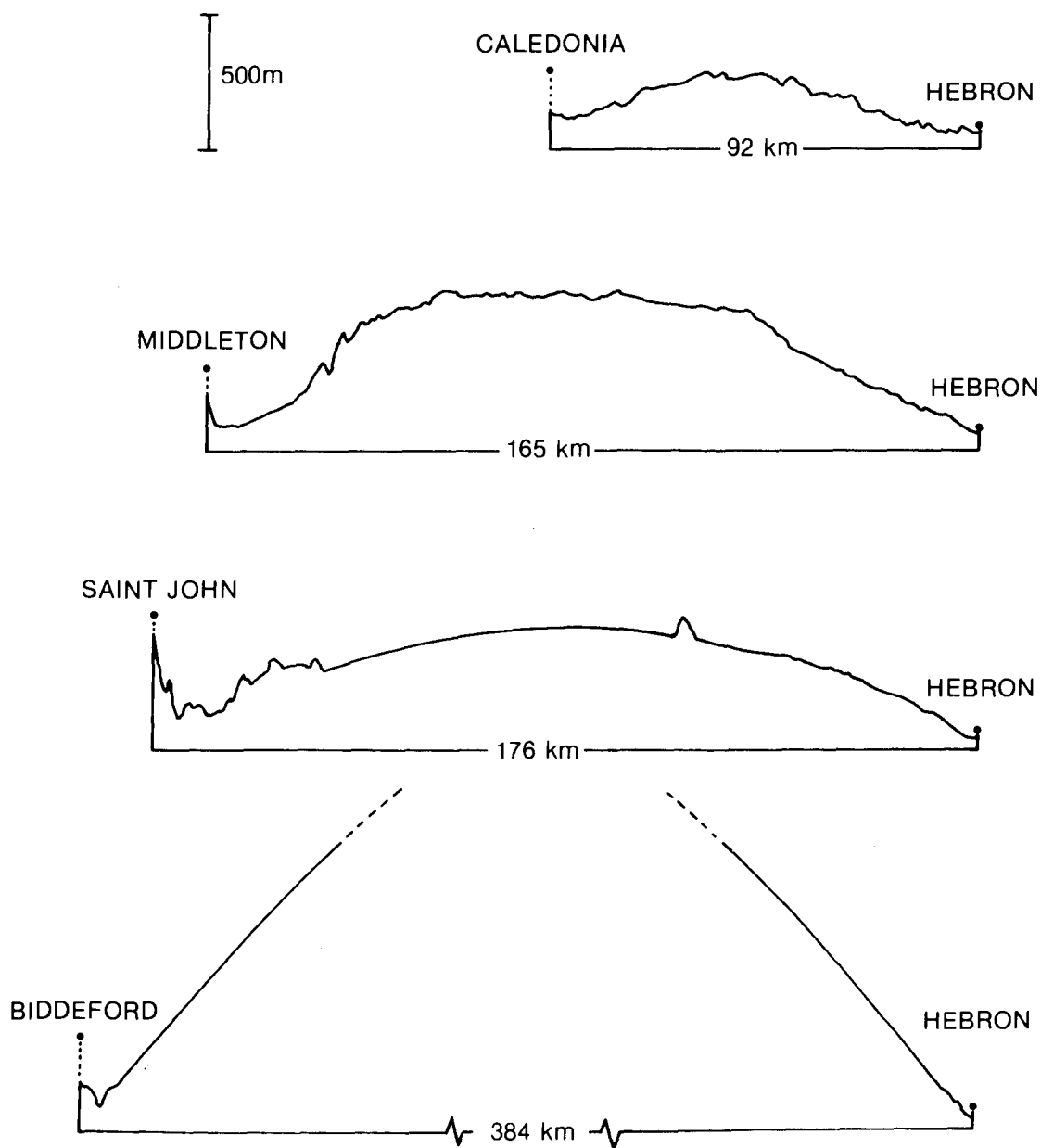


Figure 2. Profiles of the the four transmission paths, all drawn to the same scale. Four-thirds earth curvature is included. The asterisks at the end points indicate the antenna positions. The high point on the Saint John-Hebron path is Digby Neck, a peninsula on the north-west coast of Nova Scotia. The ultimate height of the obstruction on the Biddeford path is 2168 m.

1.3 PROPAGATION PATHS

The propagation paths are shown in Figures 1 and 2, and relevant parameters are given in Tables 1 and 2. There are various path lengths, frequencies, and land-water combinations. In this report, transmitters are always listed in order of increasing path length, and, for the Saint John path, in order of increasing frequency. 'Effective Distance' (d_e), a parameter defined in references 1,2, and 6, may be used to order data on the variability of received power. It combines, in a rough and arbitrary way, the effect of distance, antenna heights (or horizon distances) and frequency. In terms of effective distance, the Middleton path is longer than the Saint John path.

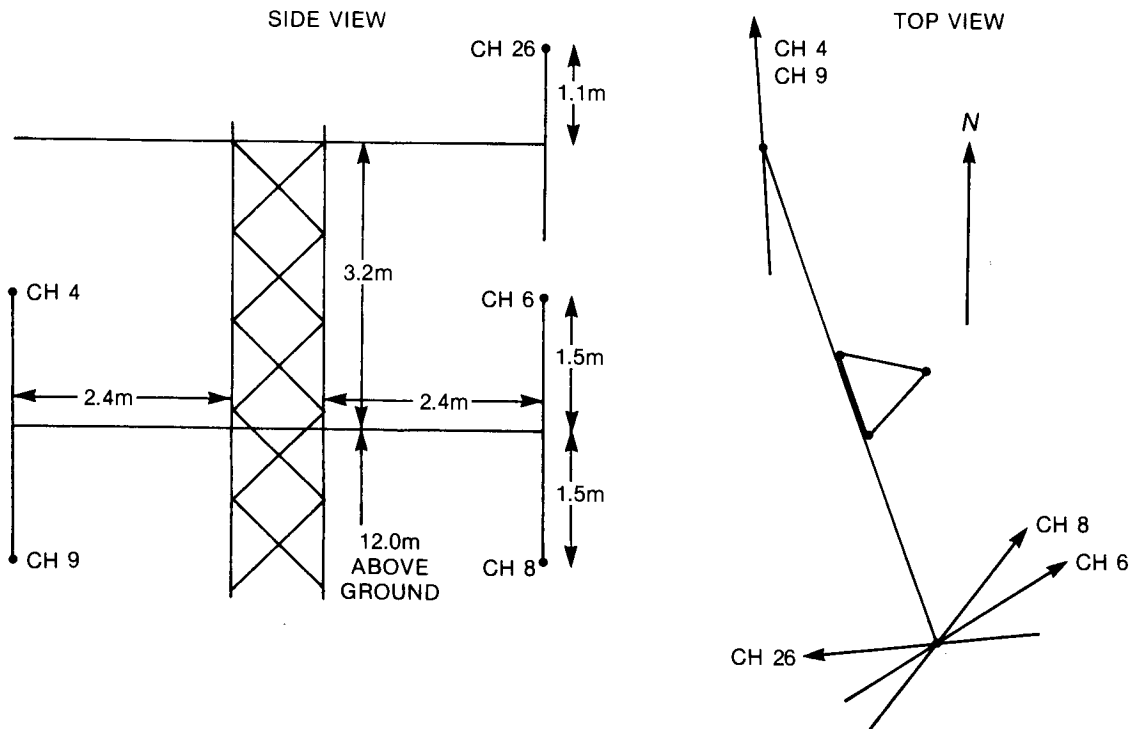


Figure 3. The arrangement of the receiving antennas on the tower at Hebron.

TABLE 3
Video Carrier Power, Gains and Losses

Name	Channel	Max ERP (kW)	Max ERP to Hebron (kW)	(dBk)	Average EIRP (dBk)	Rx Gain (dBi)	Rx Loss (dB)	C (dB)
Caledonia	6	100	100	20.0	17.3	10.2	2.0	85.5
Middleton	8	42.4	23.2	13.7	11.0	12.7	3.0	80.7
Saint John	4	100	40.0	16.0	13.3	10.2	1.8	81.7
Saint John	9	325	98.3	19.9	17.2	12.7	3.0	86.9
Biddeford	26	692	542	27.3	24.6	14.2	4.9	93.9

Note: In going from 'Max ERP to Hebron' to 'Average EIRP', 2.2 dB have been added and 4.9 dB have been subtracted.

2. EQUIPMENT FOR RECEIVING AND RECORDING

2.1 RECEIVING EQUIPMENT

Yagi antennas (Delhi J series) were used for all channels, mounted on the tower as shown in Figure 3. The number of antenna elements was 5 (channels 4 and 6), 10 (channels 8 and 9), or 15 (channel 26). The antenna gains are listed in Table 3 under 'Rx Gain'. Each antenna was connected to a receiver with 30 metres of CAC-6 75-ohm cable. The corresponding cable transmission losses are listed in Table 3 under 'Rx Loss'.

A separate fixed-frequency receiver was used for each channel, set at the video carrier frequency. In these receivers, built at CRC, frequency and bandwidth (15 kHz) are controlled by an 8-pole crystal filter. The dynamic range is 60 dB, with an approximately logarithmic response.

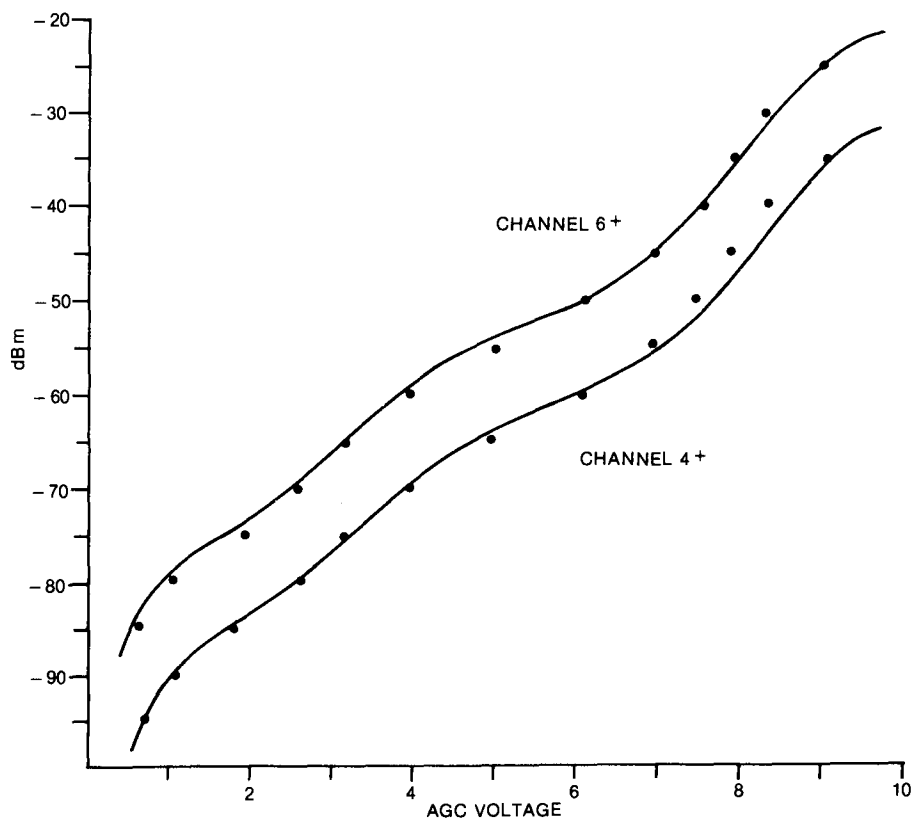


Figure 4. Calibration curves for the 67.26 MHz receiver used for the Saint John (channel 4) path, and the 83.26 MHz receiver used for the Caledonia (channel 6) path. The curves were derived from calibrations made after the experiment, while the points are calibrations made in the field in March 1981.

2.2 DATA RECORDING

The AGC voltage levels of the receivers were sampled by a microprocessor-based data logger developed at CRC, which operates in the following way: Each channel is sampled 10 times per second. The data logger records each sample by incrementing the contents of one of 128 'bins', according to the voltage of that sample. At the end of five minutes, the contents of the bins, which represent the distribution of signal levels for that five minutes, are sent to a tape recorder. In this way, the signal level can be sampled rapidly without requiring much magnetic tape. Tape cartridges were changed once per week.

For visual inspection, AGC voltage levels were also recorded on chart paper.

2.3 CALIBRATION

The data logger permits calibration of the receivers at any time by means of a signal generator. This was done at approximately weekly intervals when cartridge tapes were changed. Calibrations were also marked on the chart paper. In addition, all of the receivers were calibrated in the laboratory after the end of the monitoring period.

Figure 4 shows the laboratory post-mortem calibrations (or rather a close polynomial fit to these calibrations) for two of the receivers, and calibrations made by a CRC technician in the field early in the monitoring period. This comparison, and mass plots of the other calibrations, indicate that there was no appreciable drift during the course of the monitoring. Because of this apparent stability, and because some of the calibrations made in the field were erratic, only the post-mortem calibrations were used in the data analysis. (During two visits by CRC technicians, some receiver attenuator settings were changed. These changes were recorded, and taken into account in the comparisons mentioned above.)

3. DATA ANALYSIS

3.1 PATH LOSS

The effect of a propagation path on received power is usually expressed as 'basic transmission loss' or 'path loss'. This quantity may be found [Hall (2), p.11] from

$$L_b(\text{dB}) = \text{EIRP}(\text{dBm}) - P_r(\text{dBm}) + G_r(\text{dBi}) - L_r(\text{dB}) \quad (1)$$

where L_b is the basic transmission loss (between isotropic antennas) in decibels, EIRP is the effective isotropic radiated power of the transmitter in dBm, P_r is the power entering the receiver, also in dBm, G_r is the gain of the receiving antenna (in dB relative to an isotropic antenna), and L_r is the loss due to the cable connecting the antenna to the receiver. Since all of the terms on the right-hand side of equation (1) are constant except for P_r , it is convenient to add them together, and since transmitter power is usually measured in kilowatts, it is convenient to add to this sum the 60 dB required to convert from dBk to dBm. Then

$$L_b(\text{dB}) = C - P_r(\text{dBm}) \quad (2)$$

where

$$C = \text{EIRP}(\text{dBk}) + 60 + G_r(\text{dBi}) - L_r(\text{dB}) \quad (3)$$

Values for these quantities are given in Table 3. Later in this report, the symbol L will be used with other subscripts or no subscript to indicate various percentiles or averages, but it will always refer to the basic transmission loss defined above.

3.2 EFFECTIVE RADIATED POWER

The effective radiated power and antenna patterns for the transmitters used in this study were obtained from the regulatory branch of DOC, except for the U.S. station, for which this information was obtained from the FCC.

There are several corrections to be considered: (a) The effective radiated power (ERP) as quoted by the regulatory agencies is the power radiated by a half-wave dipole; the EIRP is 2.2 dB greater. (b) Some of the transmitting antennas are not omnidirectional. If the path in question is not at the maximum of the horizontal pattern, the effective radiated power is reduced from the quoted value. (c) All of the transmitting antennas have a vertical pattern with a pronounced maximum near the horizontal. For the paths studied here, the horizon was close to the maximum of the vertical pattern (within 1 dB), and no correction was made. (d) The power quoted by the regulatory agencies is the peak power, emitted only during the synchronizing pulse. The average carrier power was estimated from prescribed and observed modulation patterns, as described in Appendix A. It was estimated to be 4.9 dB below the peak power.

As described in Appendix B, the ERP of three of the transmitters was verified by measurements.

3.3 HOURLY DISTRIBUTIONS

The data from two years of monitoring, transferred to 9-track (800 BPI) magnetic tape, occupy twenty-two reels of tape. To make the data more manageable, the five-minute distributions were combined to form one-hour distributions, each containing 36000 samples (ideally, for no data interruptions). The boundaries of the one-hour intervals are at integral hours, e.g. on any day there is a distribution for the time interval 1200 to 1300 Atlantic Standard Time. At this stage, the calibrations were applied, and the hourly distributions of AGC level were converted to corresponding hourly distributions of signal level in dBm. These hourly distributions were used as the basis for all subsequent analysis.

3.4 DIURNAL VARIATION

For each month during the period of observation, a distribution for each hour of the day was found by combining the distributions for that hour obtained on all the days of the month. For an ideal month of uninterrupted data collection, each such distribution contains $30 \times 36000 = 1.08$ million samples. For each month, a diurnal plot was made of the medians, and also of the 10% and 90% signal levels. Later, distributions from the same month for different years were combined. Still later, after inspection, months with similar diurnal variations were grouped into seasons, and the resulting plots are the ones shown later in this report.

3.5 DISTRIBUTION FOR ALL HOURS OF THE DAY

In combining hourly distributions (for an individual day or for many days) in order to obtain the distribution for all hours, a difficulty arises: Some of the television transmitters do not operate twenty-four hours per day. A transmitter might be silent between midnight and 0800, for example. Since there is a systematic diurnal variation, simply combining all the available data would give a result that does not represent the whole day.

Diurnal data gaps were filled in the following way: If the distribution for any hour contained fewer than 0.4 times the maximum number of samples in the set of 24 distributions, that hour was considered a 'bad' hour. A diurnal sine wave was fitted to the median received power levels of the 'good' hours. A new distribution for each 'bad' hour was synthesized by shifting the distributions from the nearest two 'good' hours so that their medians matched the sine-wave at the 'bad' hour, and then finding a time-weighted average of these distributions. This synthesized distribution was added to any distribution already present in the 'bad' hour.

With the diurnal gaps filled in, the analysis can proceed to find monthly, seasonal, and long-term distributions, and annual variations. In any combination of distributions from different hours of the day or from different months of the year, the component distributions were first multiplied by suitable factors so that, before addition, they all had equal populations.

4. LONG-TERM MEDIAN PATH LOSS

4.1 MEASURED PATH LOSS

The measured values of long-term median path loss are displayed in Table 4, along with the long-term 90% and 10% path losses relative to the median. The q percentile is the path loss that represents the received power exceeded $q\%$ of the time. In other words, the path loss is less than the given value $q\%$ of the time. Sometimes the long-term median of hourly medians is quoted instead of the long-term median of sampled signal levels. These medians were also found for the Hebron data, and were found to be within 1 dB of the values shown in Table 4.

TABLE 4
Long-Term Path Loss

Name	Channel	Path		Path Loss (dB)		
				90%	50%	10%
Caledonia	6	land	82 km	+5.6	151	-6.0
Middleton	8	land	165 km	+7.9	196	-13.8
Saint John	4	mixed	176 km	+7.2	163	-12.0
Saint John	9	mixed	176 km	+7.5	184	-14.7
Biddeford	26	sea	384 km	+10.3	195	-33.9

4.2 PREDICTED MEDIAN PATH LOSS

Predictions are displayed in Table 5. The calculations were done with a computer program described by Palmer (10), using a topographic data base described by Whitteker (11). For each path, a path loss was calculated for both the diffraction mode of propagation (10) and the tropospheric scatter mode (1). The combined path loss is dominated by the mode with the lesser loss. As shown by Table 5, the diffraction mode dominates on the shortest path, the scatter mode dominates on the longest path, and the two modes are of comparable strength on the other paths.

TABLE 5
Predicted Median Path Losses

Name	without	with trees		error (dB)
	trees	distant + near		
	(dB)	error (dB)	(dB)	(dB)
Caledonia 6	142(142,168)	-9	146(146,170) + 4 = 150	-1
Middleton 8	174(177,179)	-22	185(186,192) + 11 = 196	0
Saint John 4	153(155,158)	-10	153(155,160) + 4 = 157	-6
Saint John 9	162(164,167)	-22	165(166,183) + 11 = 176	-8
Biddeford 26	198(222,198)	+3	198(222,198) + 0 = 198	+3

Note: Each 'nnn(nnn,nnn)' signifies 'combined loss (diffraction,scatter)'.

Since the heights of the antennas at the Hebron site were comparable with the heights of nearby trees, foliage attenuation must be considered. Otherwise the path loss is underestimated by about 20 dB for the paths that terminate on the two lowest antennas (see Figure 3). Because the measured transmission loss on these two paths was so much higher than at first predicted, the author made measurements of the ERP of the transmitters, and of the field at Digby Neck due to the transmitters at Saint John across the Bay of Fundy. The results are described in Appendix B. Briefly, it was found that the transmitters were emitting at the powers that had been assumed, and that the intensity arriving at Digby Neck was as calculated. Therefore the excess attenuation was due to some aspect of the land portion of the paths, most likely the trees surrounding the receiving site.

The calculation 'with trees' takes trees into account in two ways: For trees more distant than 250 m from the receiving site, the height of the land is increased by 10 to 20 metres, depending on frequency. (Trees look more opaque at higher frequencies (13).) For most paths, this has little effect, but toward Middleton, where the terrain rises gradually to a hill 7 km distant, the extra attenuation amounts to 11 dB. Nearby trees may be regarded as clutter (10,13). The size and shape of the clearing at Hebron was estimated from an aerial photograph, and the height of the trees estimated from local photographs. Typically the trees (mostly coniferous) were estimated to be 80 m distant and 12 m high. Table 5 shows the result. The agreement between calculation and observation is adequate, given that detailed path-loss predictions for irregular terrain have an rms error about 6 dB (10), and that estimates of foliage attenuation are subject to much larger errors.

5. VARIATION OF SIGNAL — TIME SERIES

5.1 TIME SERIES OF HOURLY MEDIANS

Plots of time series of hourly median values of path loss are shown in Figures 5 to 11. These particular months provide an approximately uniform coverage of the seasons, while avoiding the worst data gaps. The data shown in these figures are in their least processed form in this report.

The time-series plots will not be discussed in detail, but the reader may obtain from them a general impression of how signal strength varies. Some examples: There is an obvious diurnal variation some of the time, e.g. Middleton, March; Caledonia, July. Often there is a correlation between the variations of the signal on different channels, e.g. during the first half of April 1981. It might be possible to relate such events to meteorological changes, but this has not been attempted in this study. In summer, the variations on the long over-ocean path from Biddeford sometimes exceed the dynamic range (60 dB) of the receiver.

5.2 AUTOCORRELATION OF TIME SERIES

Figures 12 and 13 show the autocorrelation of hourly medians for two of the months displayed in the time-series plots. They show that the autocorrelation drops to 0.5 in a period of from 3 to 9 hours, depending on channel and season. In other words, individual excursions of received power do not usually last more than a few hours. Beyond that time, some of the curves, notably the one for Caledonia, display a positive day-to-day correlation.

5.3 ONE-YEAR PLOTS OF DAILY MEDIANS

Figures 14 and 15 show the general behaviour of the signal level over the whole period of observation. Parts of 1981 and 1983 have been put together on one plot. The gaps in data show where equipment malfunctions occurred, usually involving the recording equipment rather than the receivers. Daily medians for individual days were found by the method described in section 3.5. If, on a given day, the transmitter was off for more than 12 hours, no point was plotted for that day. During parts of the year and particularly in summer, Biddeford, an educational station, broadcast for more than 12 hours per day only on weekends, a schedule that results in a sparse plot during such periods. In these one-year plots, the annual variations that are the subject of further analysis are already evident.

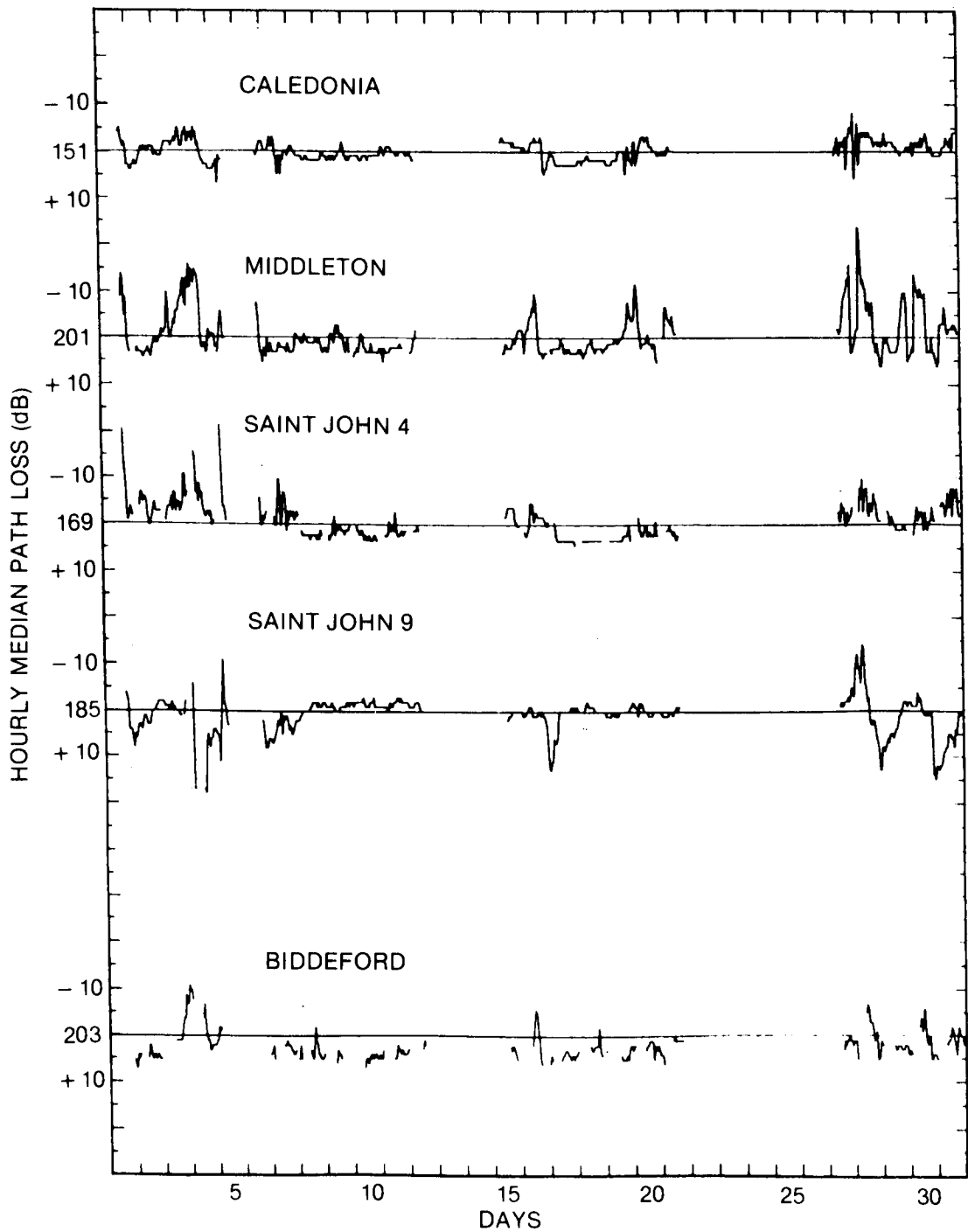


Figure 5. Hourly median values of path loss for January 1982. For each path, the monthly median is represented by a horizontal line; its value is given on the left. Path loss increases downward; received power increases upward.

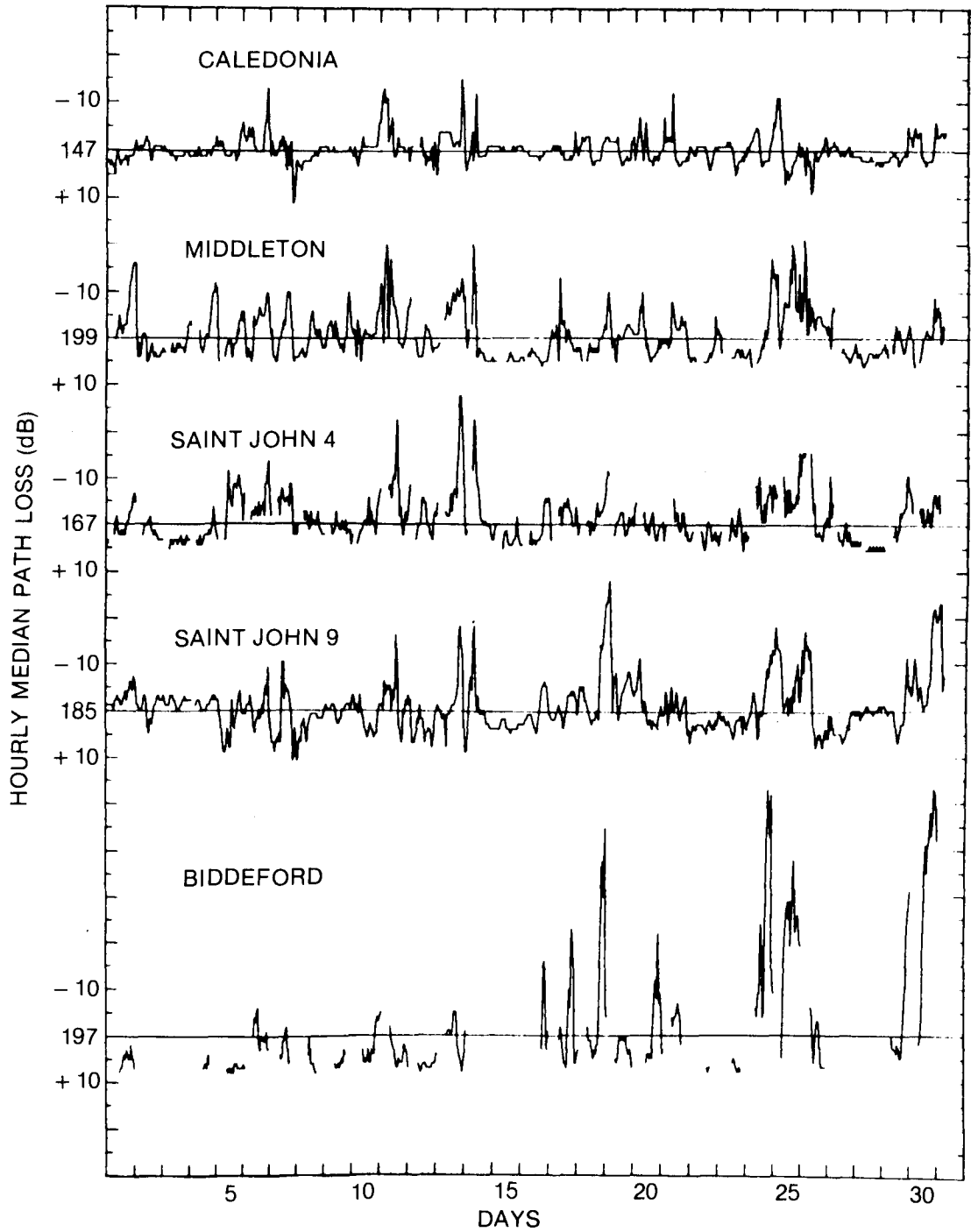


Figure 6. Hourly median values of path loss for March 1982. For each path, the monthly median is represented by a horizontal line; its value is given on the left. Path loss increases downward; received power increases upward.

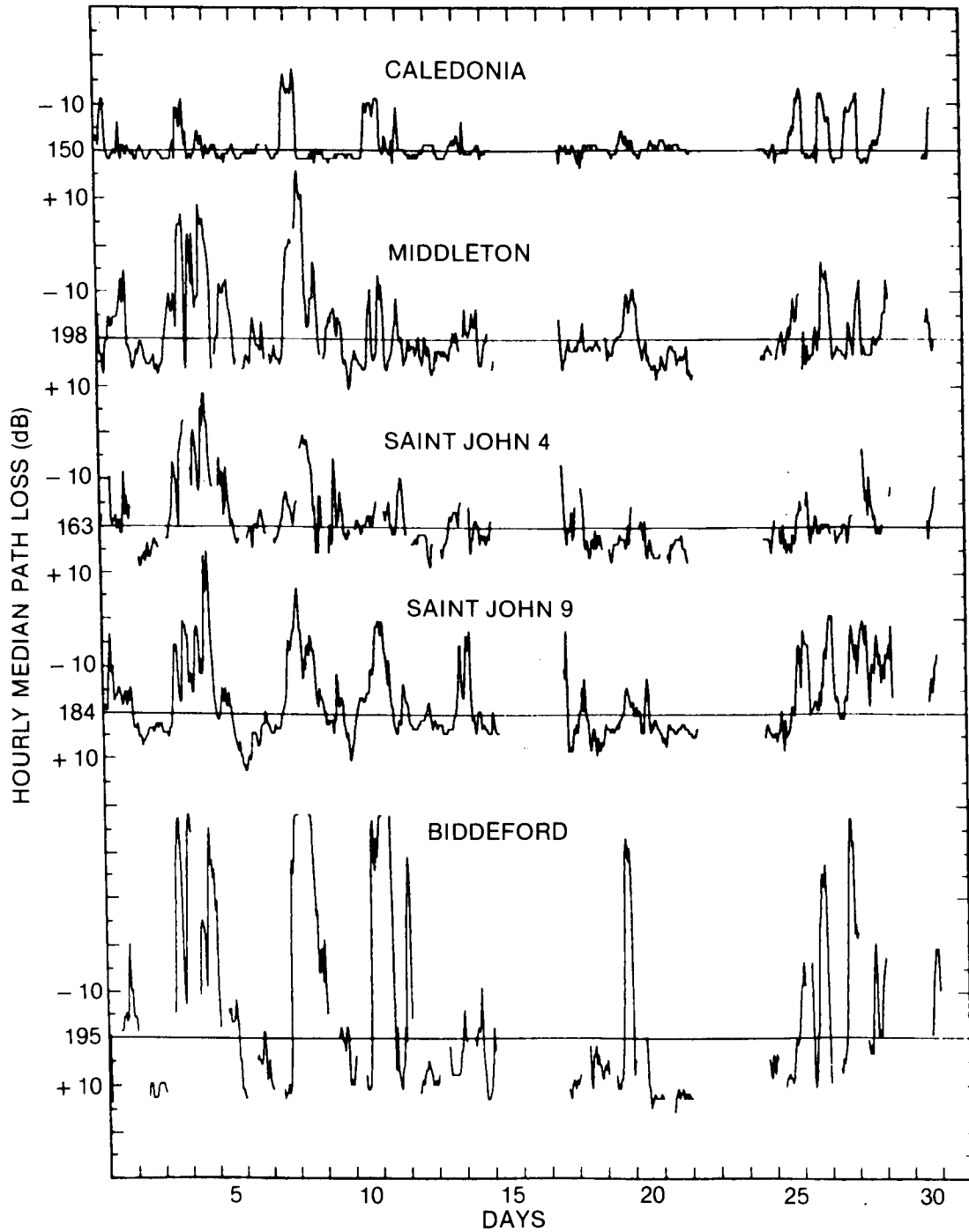


Figure 7. Hourly median values of path loss for April 1981. For each path, the monthly median is represented by a horizontal line; its value is given on the left. Path loss increases downward; received power increases upward.

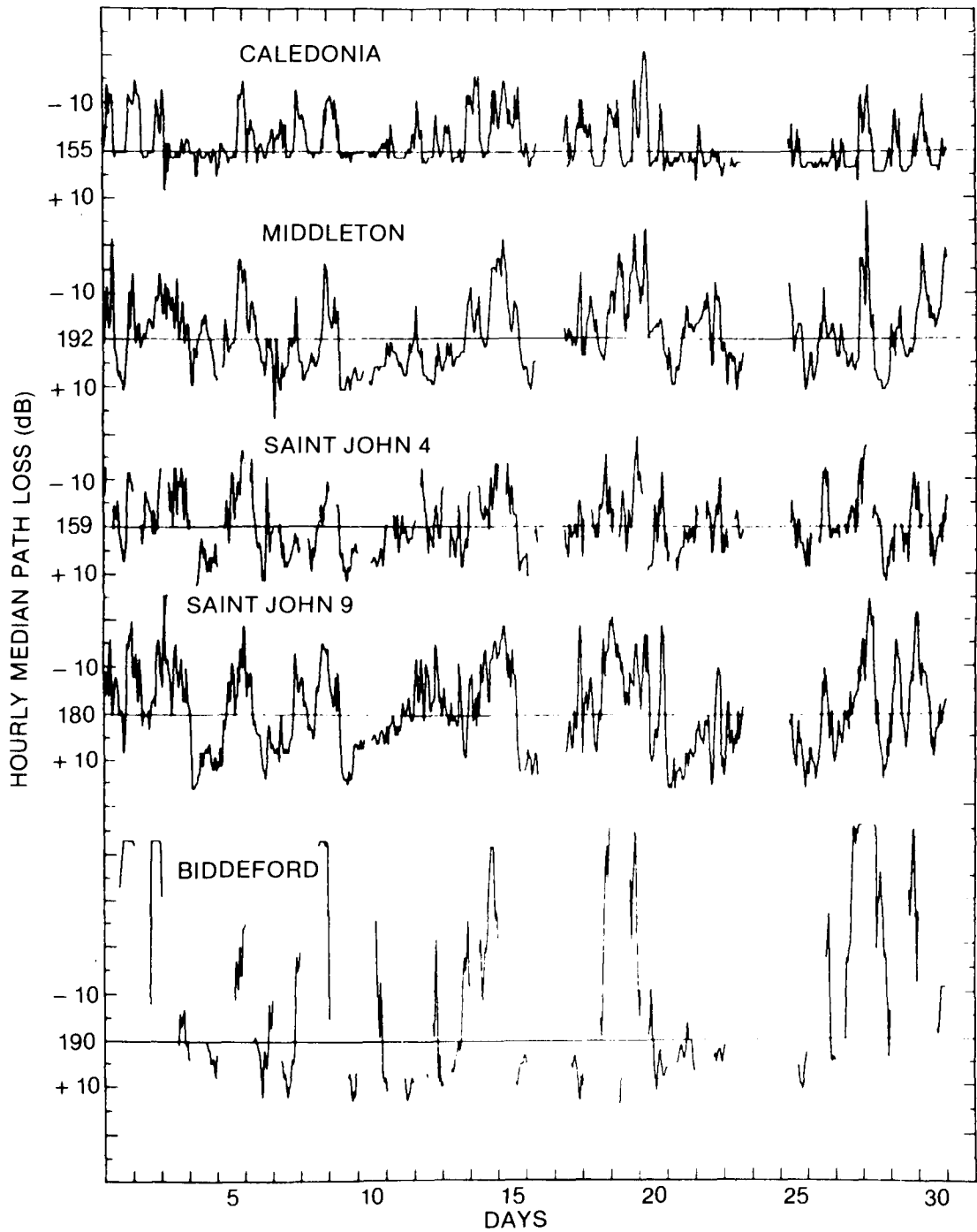


Figure 8. Hourly median values of path loss for June 1981. For each path, the monthly median is represented by a horizontal line; its value is given on the left. Path loss increases downward; received power increases upward.

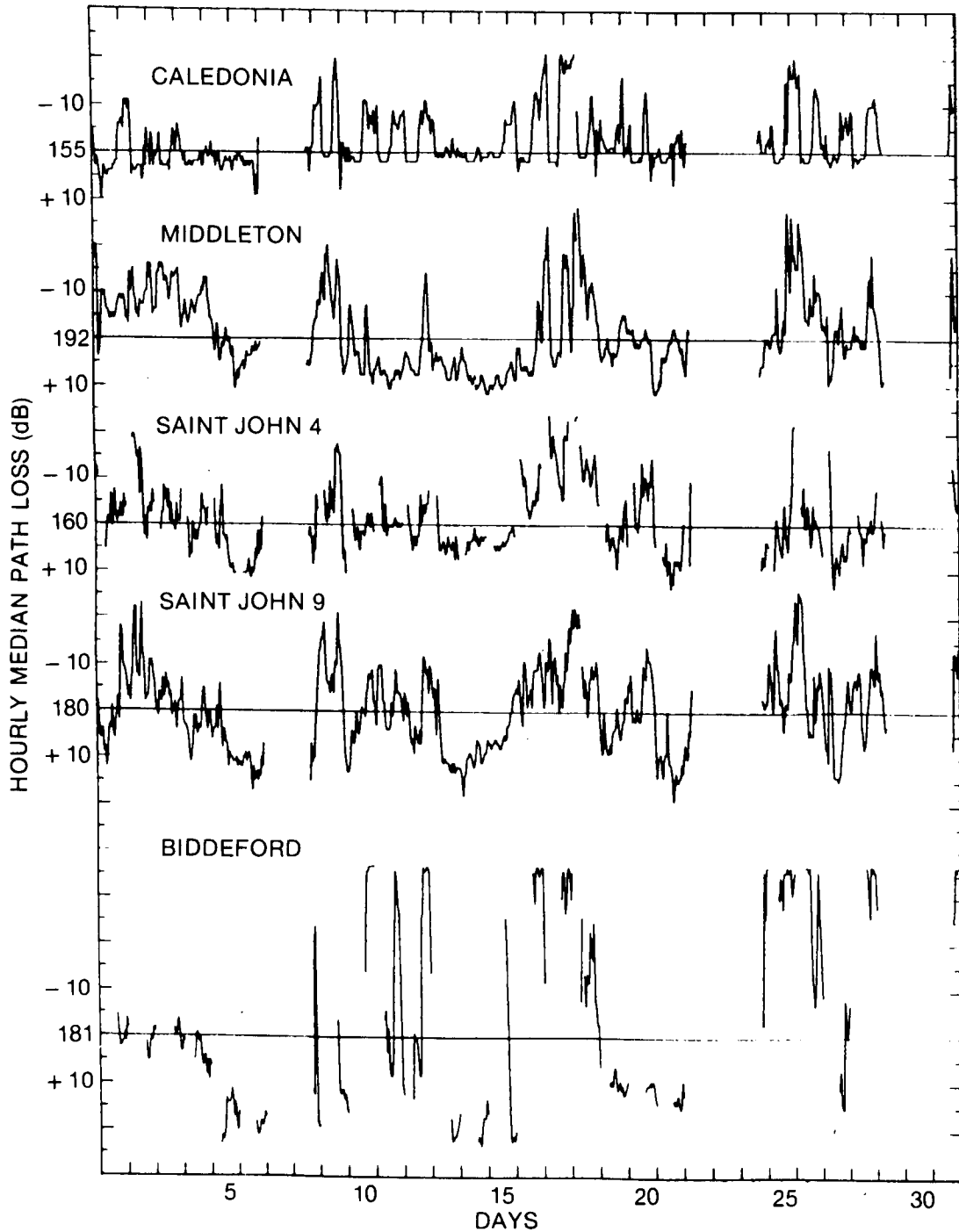


Figure 9. Hourly median values of path loss for July 1981. For each path, the monthly median is represented by a horizontal line; its value is given on the left. Path loss increases downward; received power increases upward.

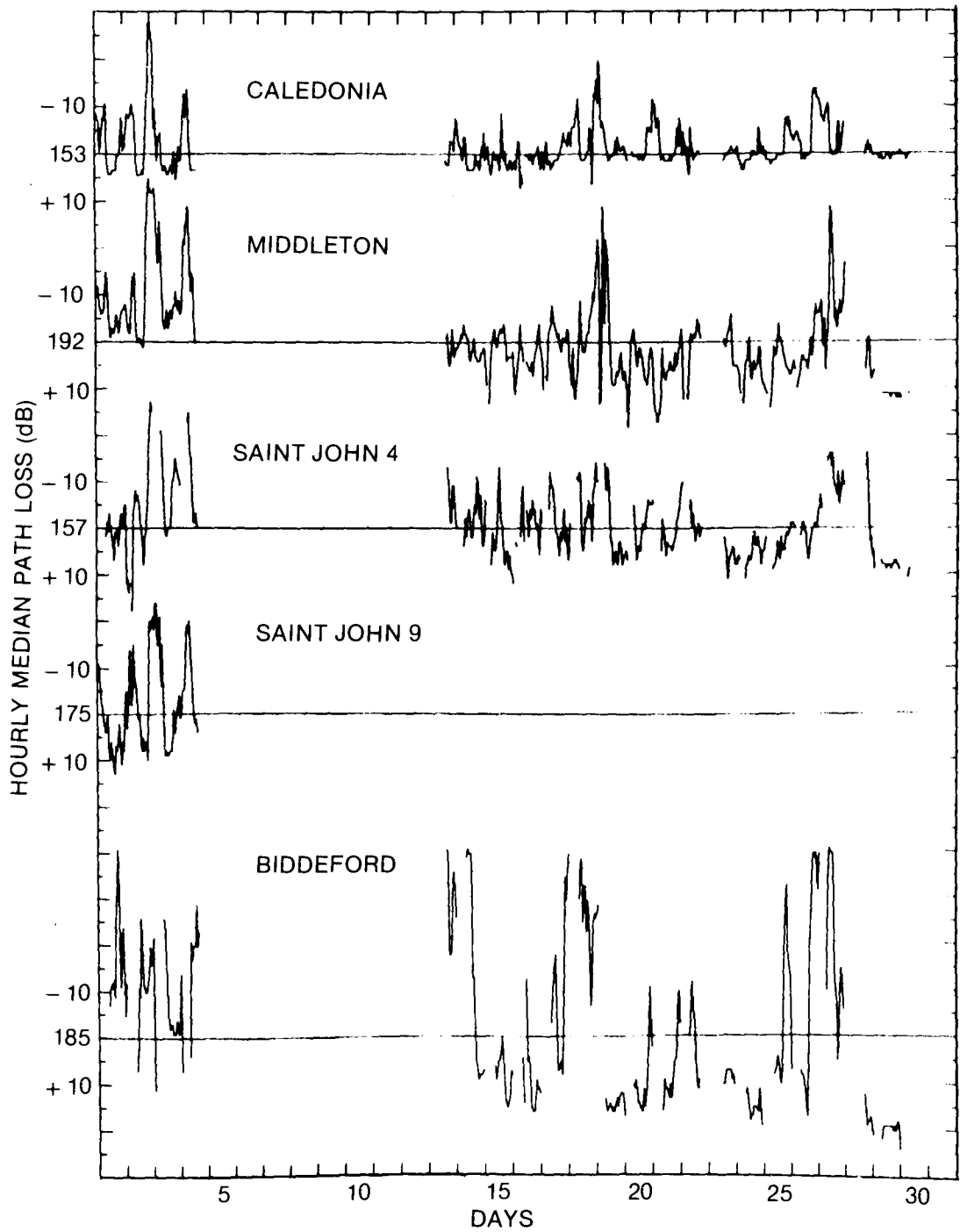


Figure 10. Hourly median values of path loss for September 1981. For each path, the monthly median is represented by a horizontal line; its value is given on the left. Path loss increases downward; received power increases upward.

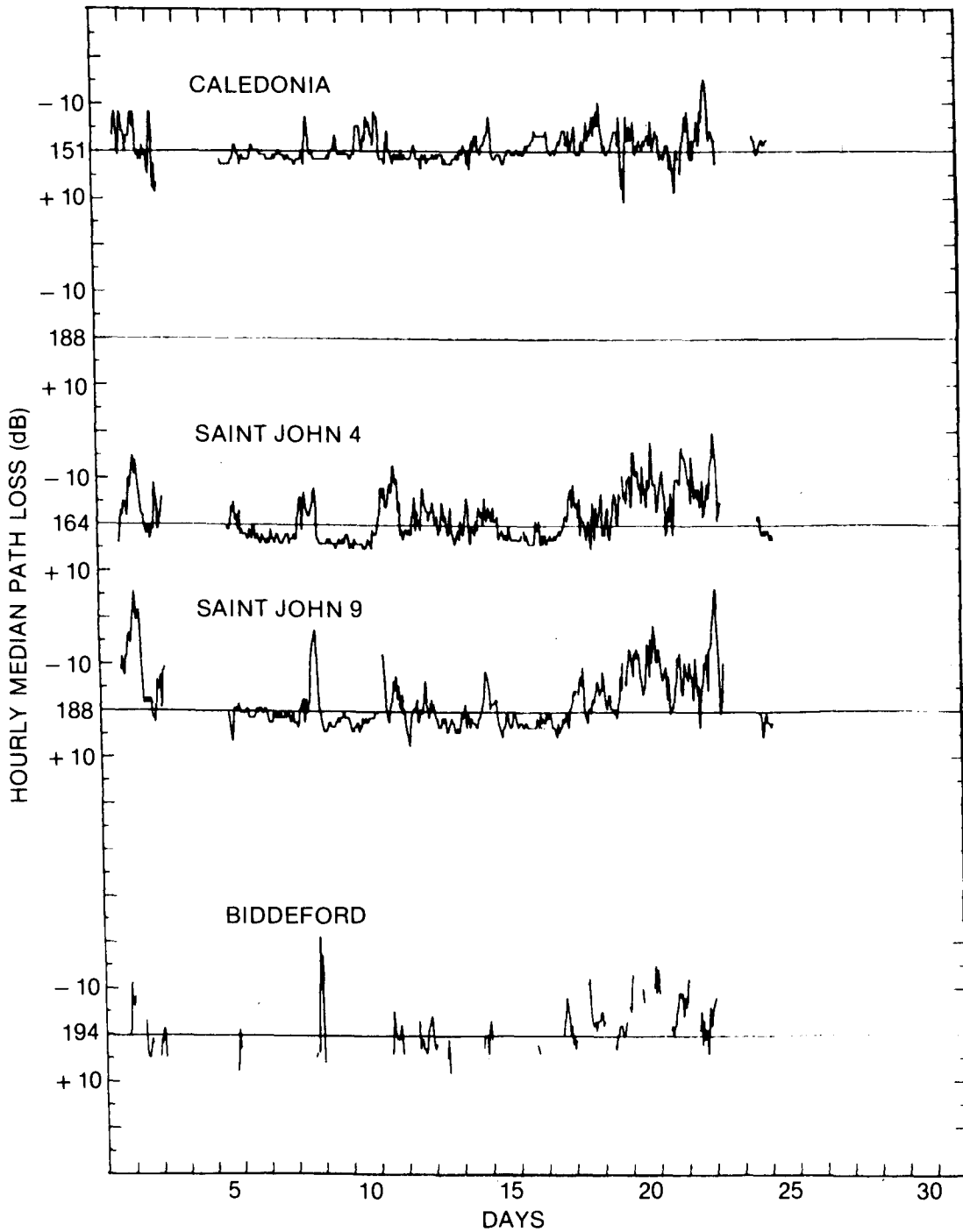


Figure 11. Hourly median values of path loss for November 1982. For each path, the monthly median is represented by a horizontal line; its value is given on the left. Path loss increases downward; received power increases upward.

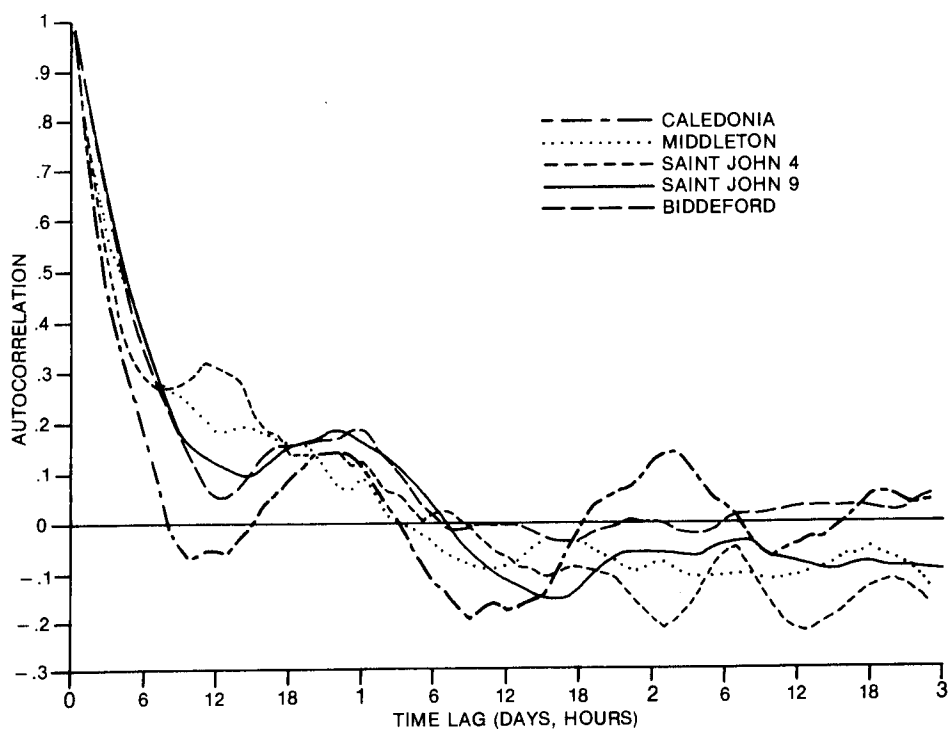


Figure 12. Autocorrelation function of hourly median values of path loss (or of received power) for all five propagation paths during March 1982. The curves are derived from the data displayed in Figure 6.

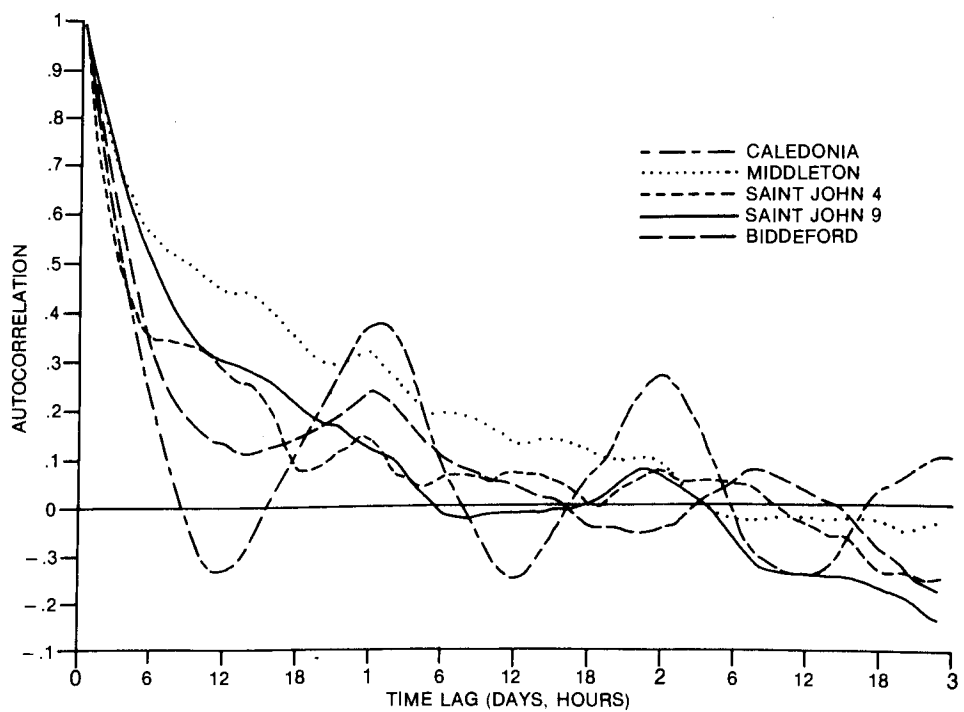


Figure 13. Autocorrelation function of hourly median values of path loss (or of received power) for all five propagation paths during July 1981. The curves are derived from the data displayed in Figure 9.

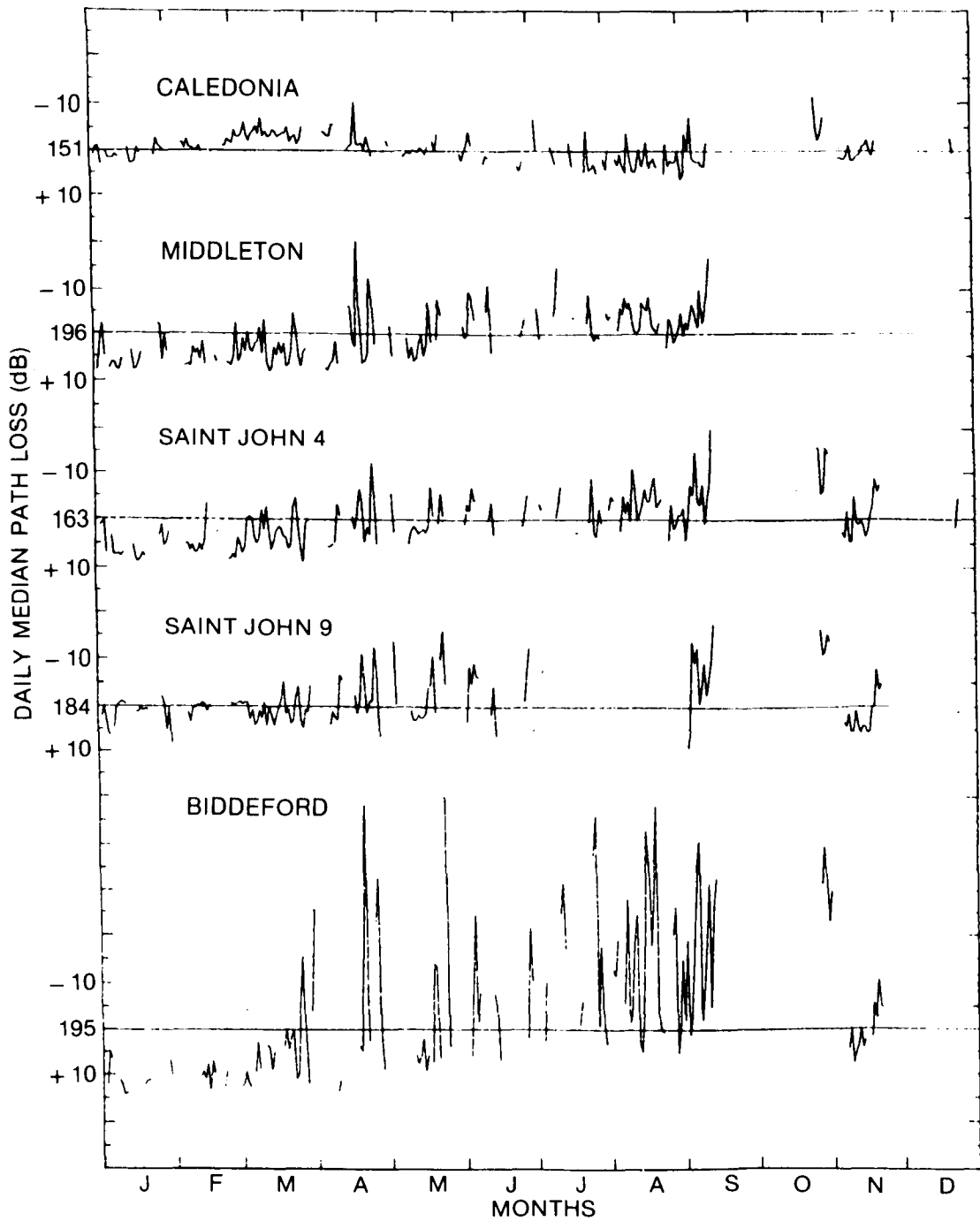


Figure 14. Daily median values of path loss for 1982. For each path, the long-term (two-year) median is represented by a horizontal line; its value is given on the left. Path loss increases downward; received power increases upward.

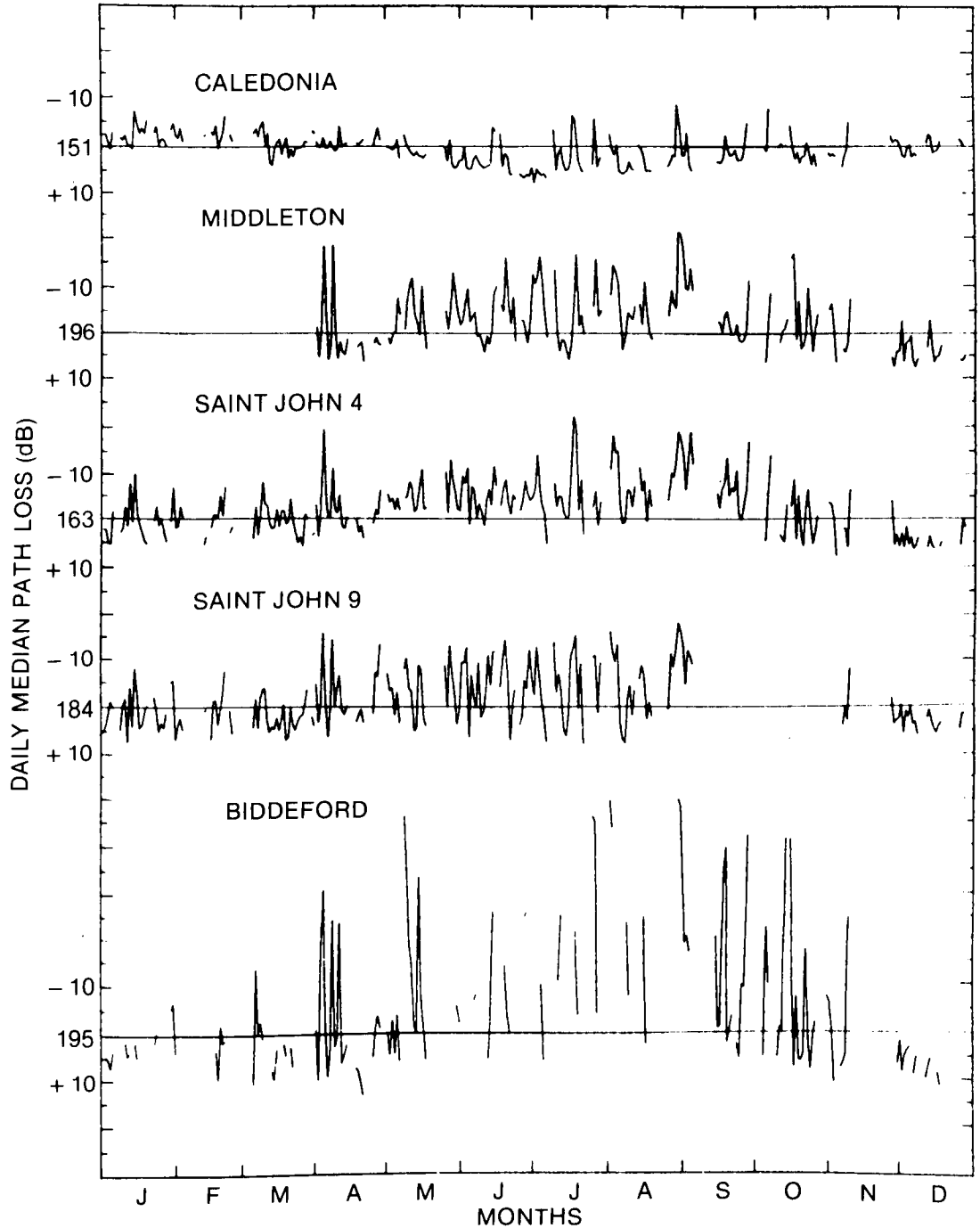


Figure 15. Daily median values of path loss for 1983 (January-March) and 1981 (April-December). For each path, the long-term (two-year) median is represented by a horizontal line; its value is given on the left. Path loss increases downward; received power increases upward.

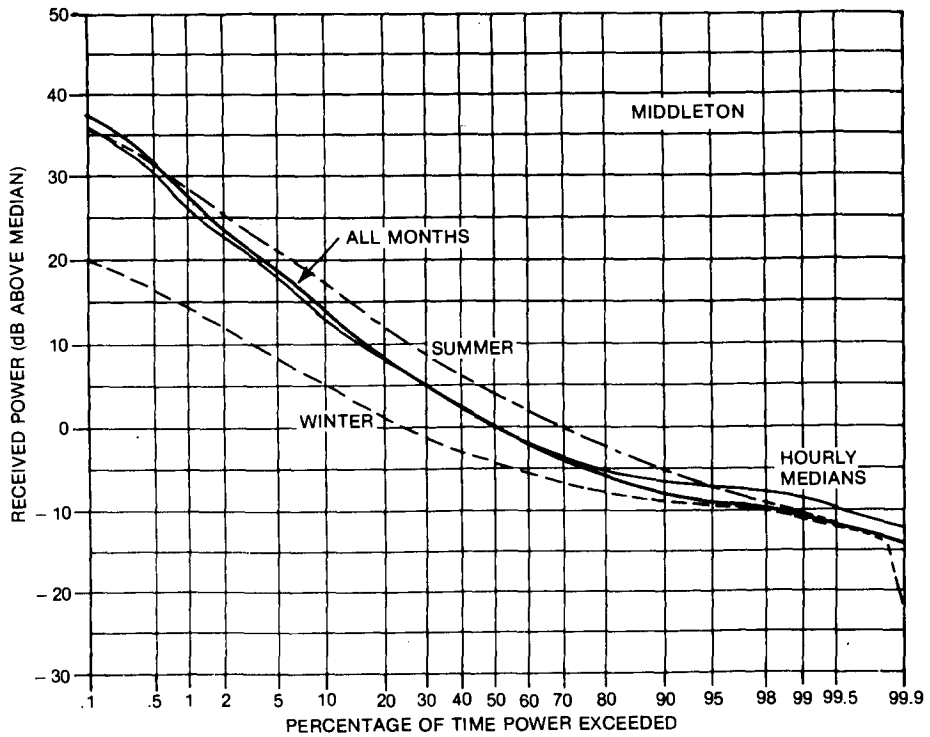
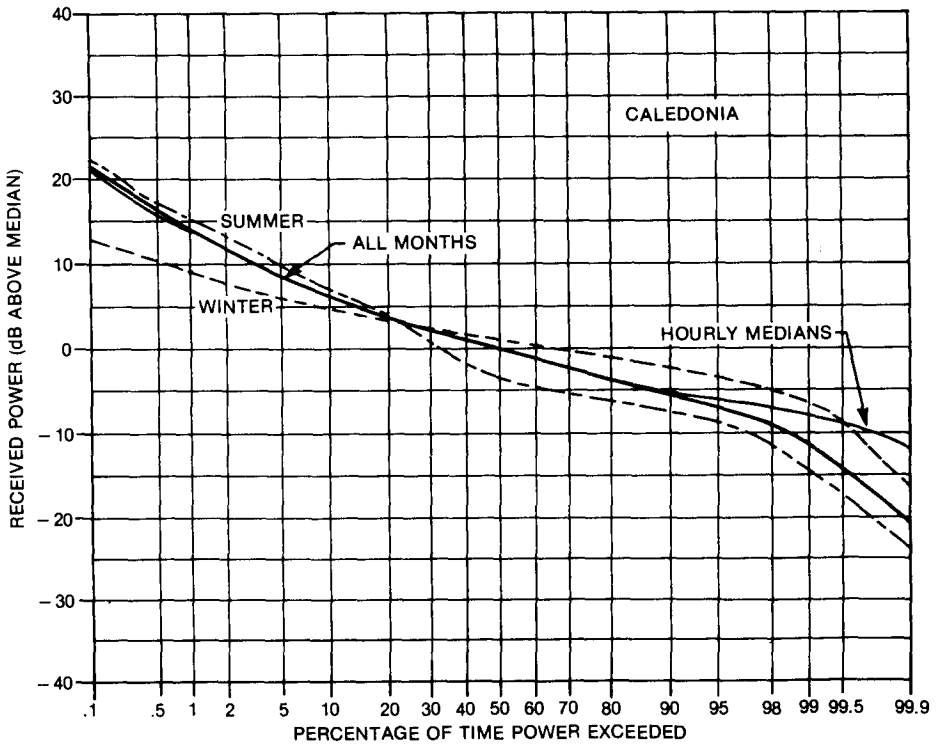


Figure 16. Cumulative distributions of power received from Caledonia and from Middleton, relative to the long-term median. The thick solid line represents the long-term distribution. The 'winter' curve is the distribution for December, January, and February; the 'summer' curve is the distribution for June, July, and August. The thin solid line represents the long-term distribution of hourly medians.

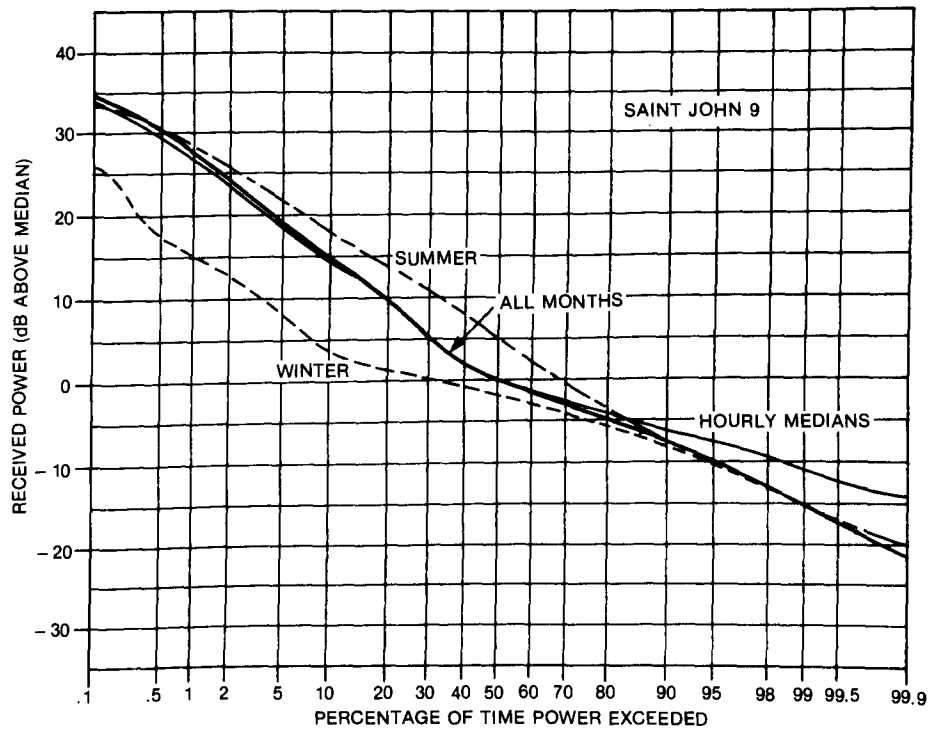
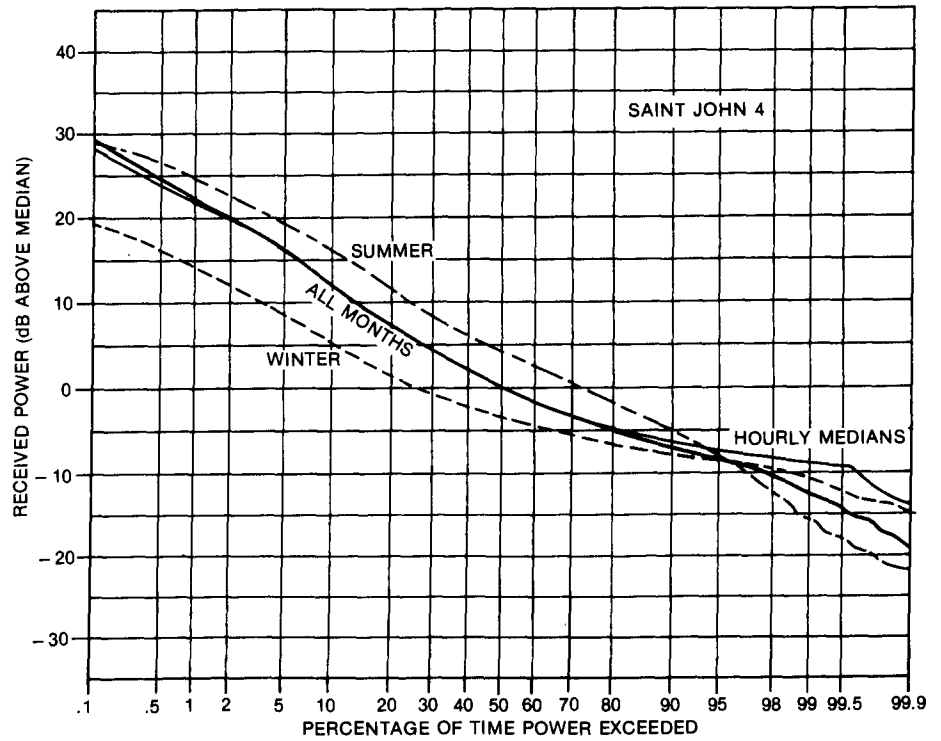


Figure 17. Cumulative distribution of power received from Saint John (channels 4 and 9), relative to the long-term median. The thick solid line represents the long-term distribution. The 'winter' curve is the distribution for December, January, and February; the 'summer' curve is the distribution for June, July, and August. The thin solid line represents the long-term distribution of hourly medians.

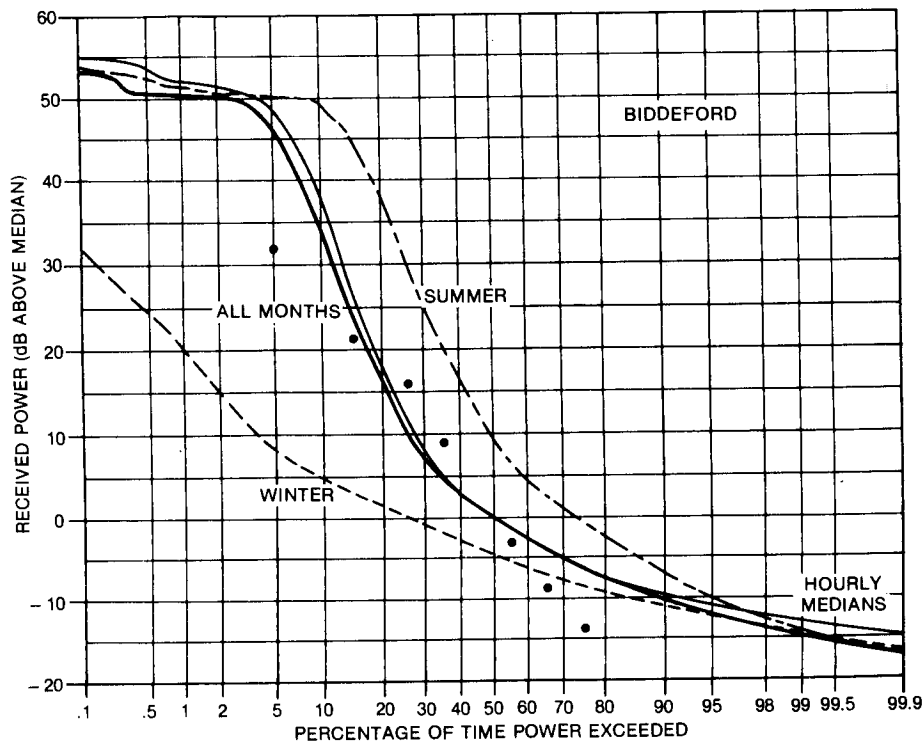


Figure 18. Cumulative distribution of power received from Biddeford, relative to the long-term median. The thick solid line represents the long-term distribution. The 'winter' curve is the distribution for December, January, and February; the 'summer' curve is the distribution for June, July, and August. The thin solid line represents the long-term distribution of hourly medians. The distributions are truncated at about 50 dB by receiver saturation. The individual points represent the path loss distribution between Sable Island and Halifax (Reference 9).

6. CUMULATIVE DISTRIBUTIONS OF RECEIVED POWER

6.1 DISTRIBUTION PLOTS

Figures 16 to 18 show the cumulative distribution of received power for each channel monitored. The long-term distribution is shown as well as the distributions for summer and winter. Plotted this way, log-normal distributions would be straight lines. Some of the distributions are approximately log-normal, but most are more complex.

In addition to the distribution based on a 0.1 s sampling interval, the long-term distribution of hourly medians is displayed. This distribution is given for comparison with the data plotted by Rice et al.(1), which are in terms of hourly medians. In almost all cases, the distribution of hourly medians is slightly narrower than the distribution of the signal level itself. The exception is Biddeford. On that path, for small percentages of the time, there tends to be a strong steady signal with occasional deep fades.

6.2 COMPARISON WITH OTHER MEASUREMENTS

The measurements reported here are only a few of many that have been made in various parts of the world at similar frequencies and distances. Figures 19 to 21 show how these results fit into summary plots from Rice et al.(1) for propagation in a maritime temperate climate. As defined by Rice et al.(1) and by CCIR (5), an oversea path is one in which the horizons of both antennas are on the sea; a path with either horizon on land is counted as an overland path. All the percentiles shown in these diagrams are from distributions of hourly medians (the thin solid lines in Figures 16 to 18).

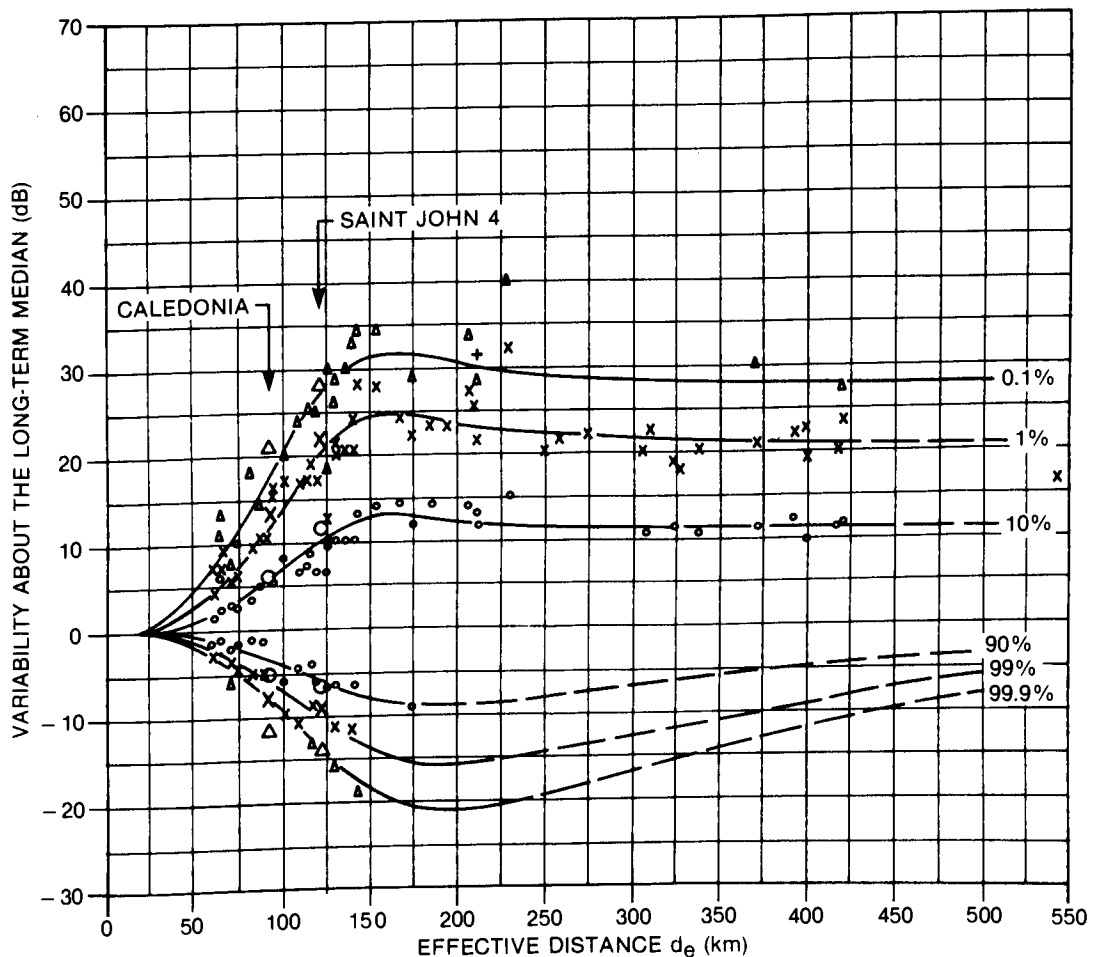


Figure 19. The variability of received signal strength (maritime temperate climate overland) in the frequency range 40-100 MHz, adapted from Figure 10.23 of Reference 1. The curves and the small plotted symbols are from the original diagram. The large symbols are from the distributions given in this report. Percentiles are represented as follows: 10%, 90% — o; 1%, 99% — x; 0.1%, 99.9% — Δ.

Since the data plotted by Rice et al. are from Britain, it is not obvious that results from the eastern coast of Canada should agree with them. Nevertheless, for VHF overland, it seems that the agreement is quite good, although the power received at Hebron, for small percentages of time may be a little greater. (The Hebron data fit the curves for a continental temperate climate about as well. The continental and maritime overland curves are not very different for $d_e < 200$ km.)

Measurements at VHF on oversea paths from Sable Island (9) are also concordant with Rice et al (1). However, there is no such agreement at UHF. On the Biddeford oversea path, the 10 percentile signal level exceeds that in Rice et al. by about 20 dB. (Because of receiver saturation, the 1% and 0.1% levels are not available from the Hebron data.) On the UHF link from Sable Island to Halifax, the 10 percentile level is also higher than the Rice et al. value, but only by 10 dB.

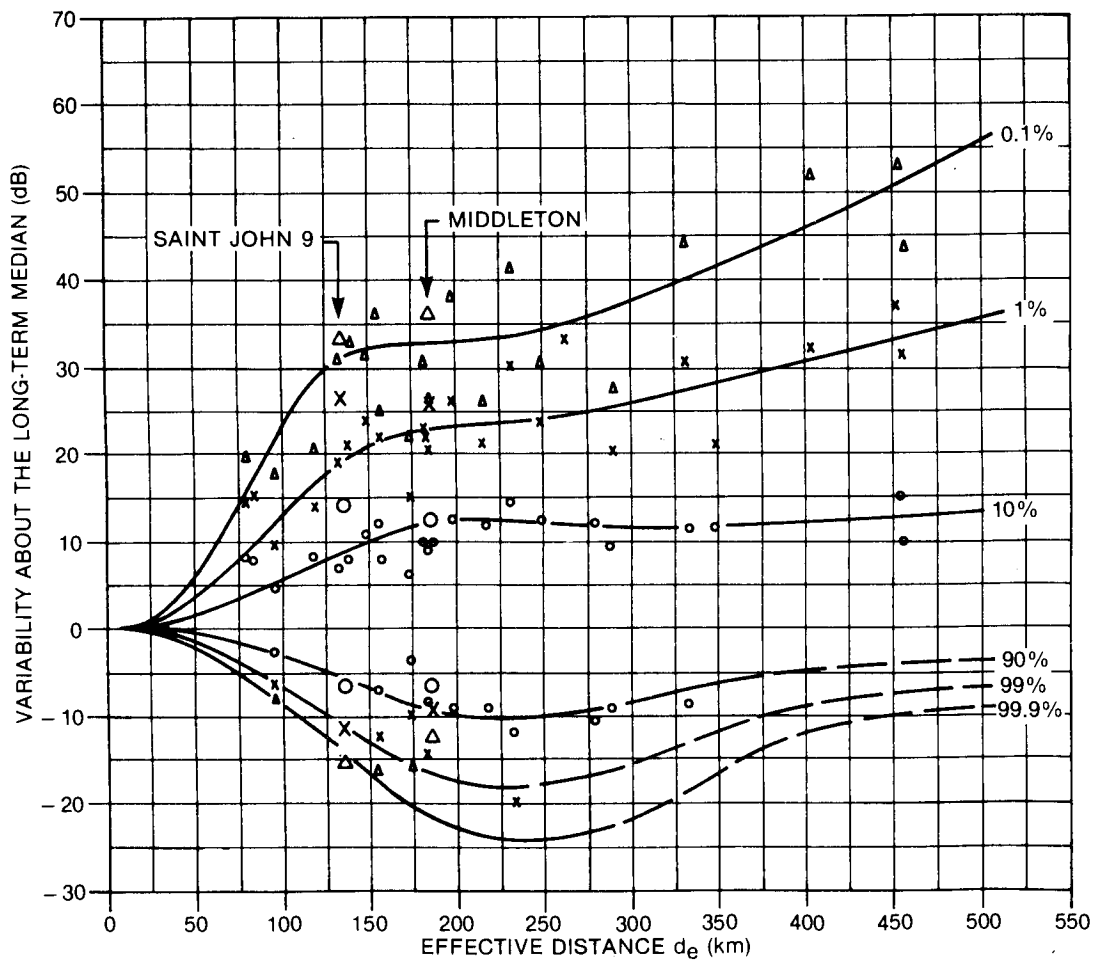


Figure 20. The variability of received signal strength (maritime temperate climate overland) in the frequency range 150–250 MHz, adapted from Figure 10.25 of Reference 1. The curves and the small plotted symbols are from the original diagram. The large symbols are from the distributions given in this report.

Since the measured distributions agree for the most part with the curves of Rice et al.(1), no new model is proposed here. In the case of UHF overseas transmission, however, those concerned with interference should be aware that the received power exceeded 10% of the time may be 10 to 20 dB greater than indicated by the Rice et al. curves.

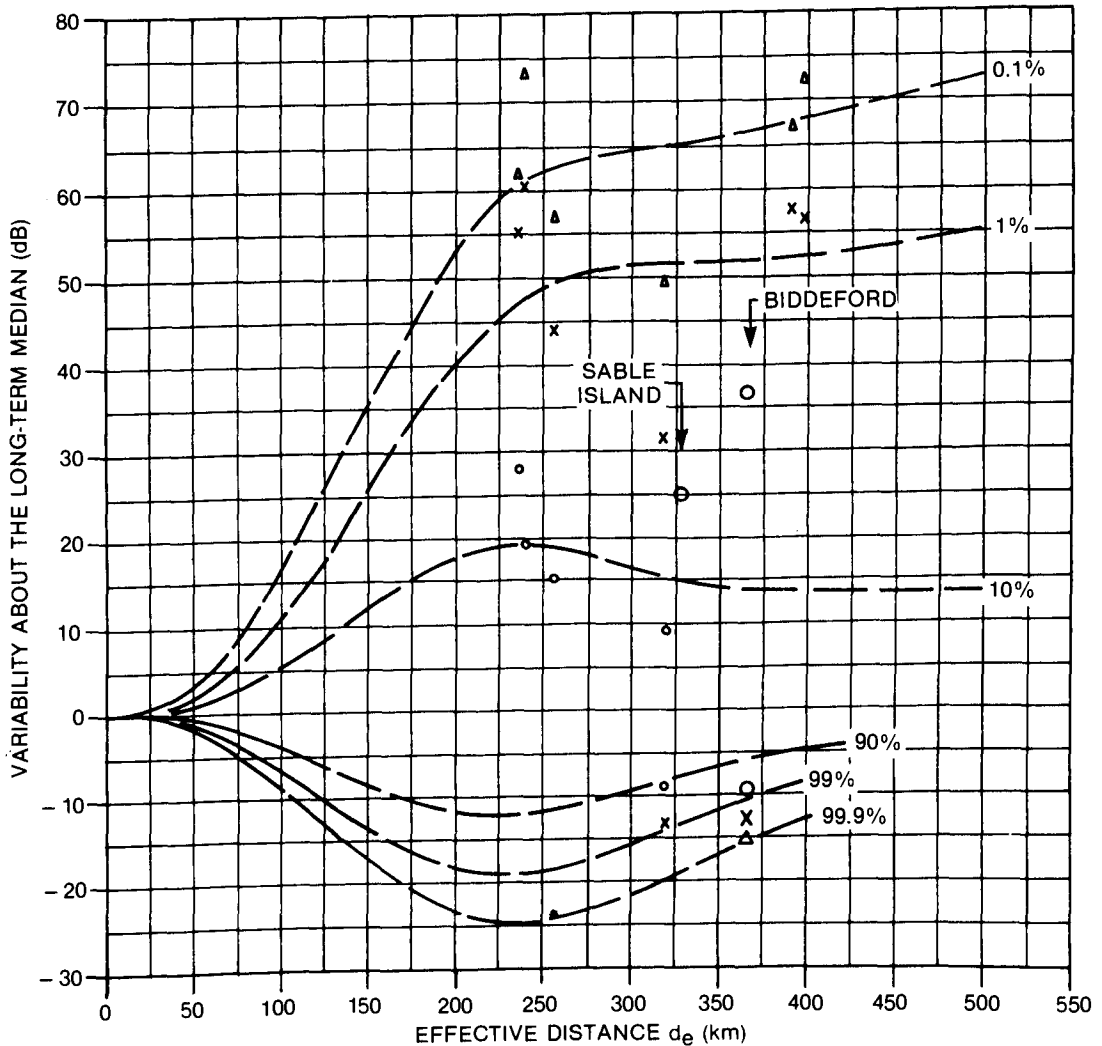


Figure 21. The variability of received signal strength (maritime temperate climate overseas) in the frequency range 450-1000 MHz, adapted from Figure 10.28 of Reference 1. The curves and the small plotted symbols are from the original diagram. The large symbols are from the distributions given in this report, except for the one labelled 'Sable Island', which is from Reference 9.

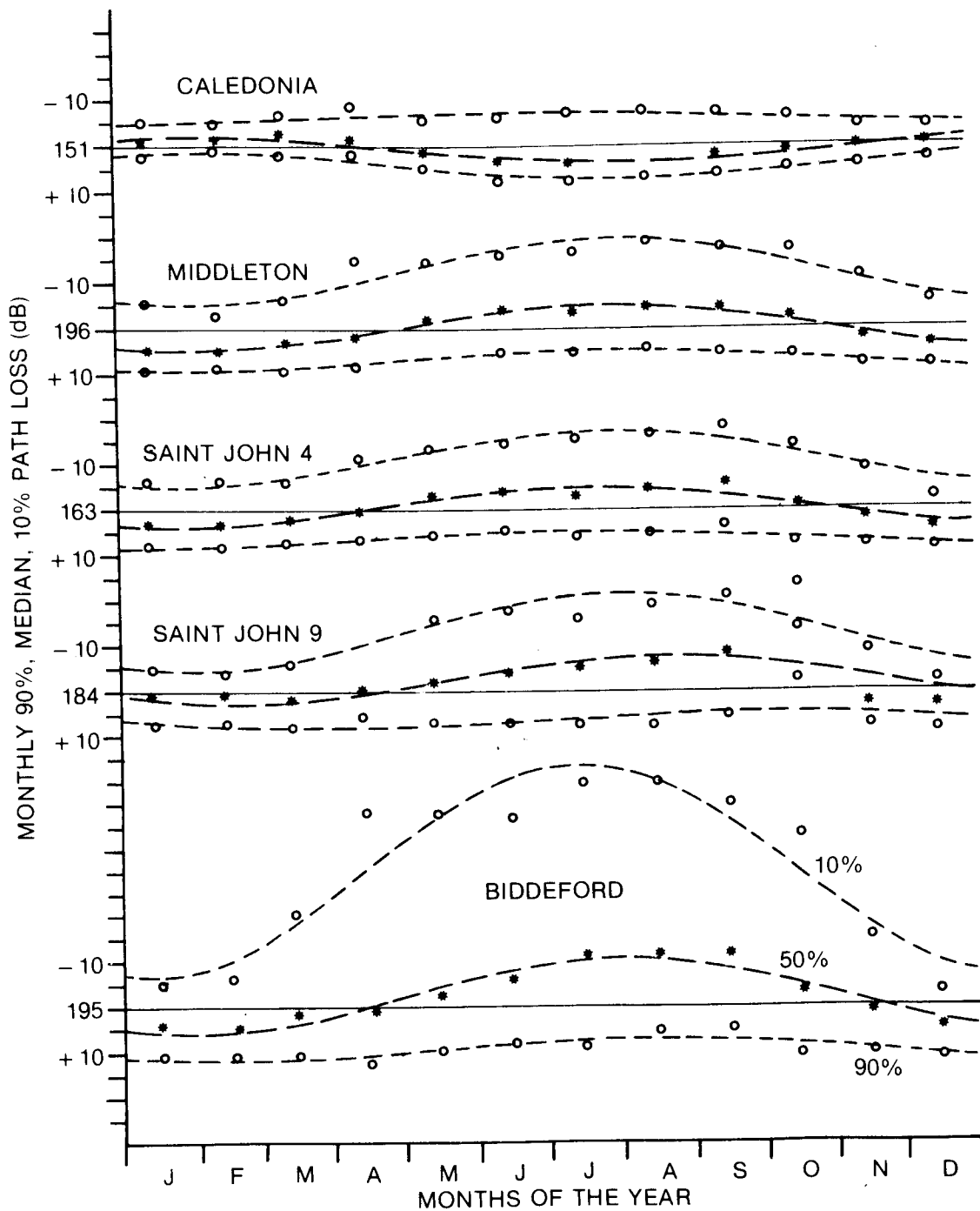


Figure 22. Annual variation of path loss. As in previous figures, the horizontal lines and accompanying numerals represents long-term median values. For each month, the asterisk represents the median, the circle above represents the 10 percentile, and the circle below represents the 90 percentile. Data from the two years of observation are combined. The curves are sine-wave fits to the points.

7. ANNUAL VARIATION

7.1 OBSERVATIONS

Percentiles from the monthly distributions are plotted together in Figure 22. The curves that have been fitted to the points are given by

$$L_a = \bar{L}_a + A \cos[(t_d - \hat{t}_d)/58] \quad (4)$$

where L_a is the basic path loss at t_d days from the beginning of the year, \bar{L}_a is its annual mean value, A is the amplitude of the annual variation, and \hat{t}_d is the time of year (in days) of maximum path loss.

Table 6 displays the values for A and \hat{t}_d . 'Effective Distance' is introduced in section 1.3 and used in section 5.2. The 90% and 50% curves for Caledonia would ordinarily be specified by a positive amplitude and phase different by 180° . Instead, in order to preserve the approximate equality of all the phases in the table, the amplitudes are given as negative.

TABLE 6
Annual Variation

Effective Distance d_e (km)	90%			50%			10%			
	Mean $\bar{L}_a - L_{it}$ (dB)	Amp. A (dB)	Phase \hat{t}_d (days)	Mean $\bar{L}_a - L_{it}$ (dB)	Amp. A (dB)	Phase \hat{t}_d (days)	Mean $\bar{L}_a - L_{it}$ (dB)	Amp. A (dB)	Phase \hat{t}_d (days)	
Cal	91	-1.3	-3.1	38	0.7	-2.7	38	-0.2	1.4	-7
Mid	186	-0.9	2.3	31	0.0	5.0	30	1.5	7.3	32
St4	121	-0.7	1.8	16	-0.6	4.4	22	0.6	6.3	27
St9	137	-0.2	0.5	-4	-1.4	4.4	27	2.3	8.3	23
Bid	366	-0.8	2.4	45	-2.5	8.3	31	3.8	23.6	13

Note: \bar{L}_a is given relative to L_{it} , the long-term percentile.

7.2 MODEL OF RESULTS

This section provides formulas that summarize the observed annual variation. These formulas are simple, and approximate the data only roughly, since the small number of propagations paths in the study does not warrant a more elaborate representation.

7.2.1 Time Factor

From Table 6, we may see that the phase constants for annual variation fall in or near the first month of the year; the average is 20 days. Therefore an annual cyclic factor may be constructed as:

$$c_a(m) = \cos[(m - 1)\pi/6] \quad (5)$$

where m is the month of the year.

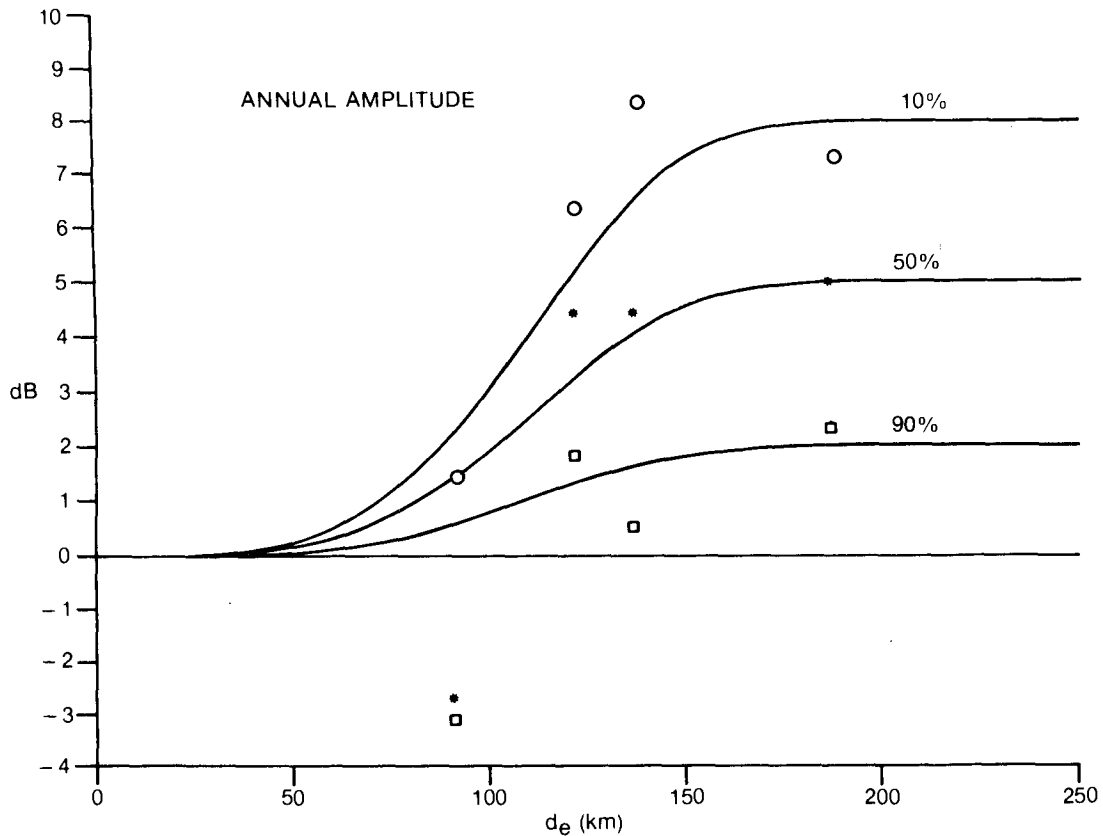


Figure 23. The amplitude of the annual variation of received power as a function of effective distance, for overland and mixed paths. The points are obtained from Table 6. The percentiles 10, 50, 90 are represented by circles, asterisks, squares, respectively. The curves represent the function f_1 (equation 6) multiplied by 8, 5, and 2 dB.

7.2.2 Distance Factor — Overland and Mixed Paths

From the data of this study alone, the dependence on path length can only be guessed at. Since the observed amplitude of the 50% annual variation increases with increasing effective distance d_e , and since d_e is used by References 1,2, and 6, it seems reasonable to use the same parameter here. Figure III.32 of Rice et al.(1) suggests that in a continental temperate climate at least, the amplitude of the annual variation increases to about $d_e = 200$ km, and is approximately constant beyond that. For the overland and mixed paths, the data of Table 6 are also consistent with this sort of behaviour, apart from the Caledonia path, which displays a negative annual variation for 90% and 50%. A path-length dependence that fits the observed amplitudes fairly well for overland and mixed paths is:

$$f_1(d_e) = 1 - \exp[-(d_e/120)^4] \quad (6)$$

This function is illustrated in Figure 23, along with the data.

Function f_1 accommodates the negative amplitudes at 91 km only in having a small positive value at that distance. It is not known whether the negative annual variation is characteristic of propagation over that distance, or whether it is due to some unsuspected peculiar feature of the Caledonia path, e.g. variable attenuation by deciduous trees.

Boithias (reference 3, p.190) suggests that the annual variation is reduced on paths that are very long compared to 250 km, but this behaviour is not modelled here.

7.2.3 Model of Annual Variation — Overland and Mixed Paths

For the overland or mixed paths, the path loss in decibels for month m and percent time $q = 10, 50,$ or 90 may then be approximated as:

$$\begin{aligned} L_1(m, 10) &= L(10) + f_1(d_e) [2 + 8c_a(m)] \\ L_1(m, 50) &= L(50) + f_1(d_e) [0 + 5c_a(m)] \\ L_1(m, 90) &= L(90) + f_1(d_e) [-1 + 2c_a(m)] \end{aligned} \quad (7)$$

where $L(q)$ is the long-term q percentile path loss. For $q = 10$ and 90 , the mean of the annual variation is different from the long-term path loss. This difference arises from the fact that some of the variance in the long-term distribution has been removed by specifying a particular time of year.

7.2.4 Model of Annual Variation — Oversea Paths

For oversea paths, we have only the data from one path and the results from Sable Island (9). The Sable Island results are for paths of 207 and 292 km at 148 MHz, and 292 km at 432 MHz. The annual variations of path loss for these paths have the same phase (within one month) as the Biddeford-Hebron path, and the amplitude is similar. A precise comparison cannot be made because the Sable Island variation was found in terms of monthly means rather than percentiles. The equations for modelling the annual variation of oversea paths then become

$$\begin{aligned} L_1(m, 10) &= L(10) + f_1(d_e) [4 + 24c_a(m)] \\ L_1(m, 50) &= L(50) + f_1(d_e) [-2 + 8c_a(m)] \\ L_1(m, 90) &= L(90) + f_1(d_e) [-1 + 2c_a(m)] \end{aligned} \quad (8)$$

although for oversea paths, there is no observational basis for choosing the same path-length factor f_1 that was used for overland and mixed paths.

7.2.5 Other Measurements

Other reports [e.g. Boithias and Battesti (4)] agree that in temperate climates, received power is a minimum during the coldest months and a maximum during the warmest months. The phase may be reversed in desert or tropical climates. The annual range of monthly medians on the longer overland and mixed Hebron paths was found to be about 10 dB. For comparison, Rice et al (reference 1, Figure III.32) suggest 4 dB between half-year averages, Boithias (3) suggests 15 dB at 250 km, Boithias and Battesti (4) display ranges from 10 to 30 dB, and Palmer (reference 7, Table 7.1) suggests about 10 dB.

8. DIURNAL VARIATION

8.1 OBSERVATIONS

8.1.1 Plots of Diurnal Variation

Figures 24 to 28 show the diurnal variations obtained from the combined distributions for the periods indicated in the captions. The diurnal variation is more pronounced in summer than in winter, and appears to be most pronounced for the shortest path. The 10% curves vary most, the median curves only a little, and the 90% hardly at all.

Figure 29 shows the distributions of received power levels at the extremes of the diurnal variation. It is another way of looking at the data represented in Figure 24. The distributions show that at noon, the signal is steady, increasing very little above the 90% level, while in the early morning, signal enhancements are more frequent. Typically, the diurnal variation of the 90% level is small.

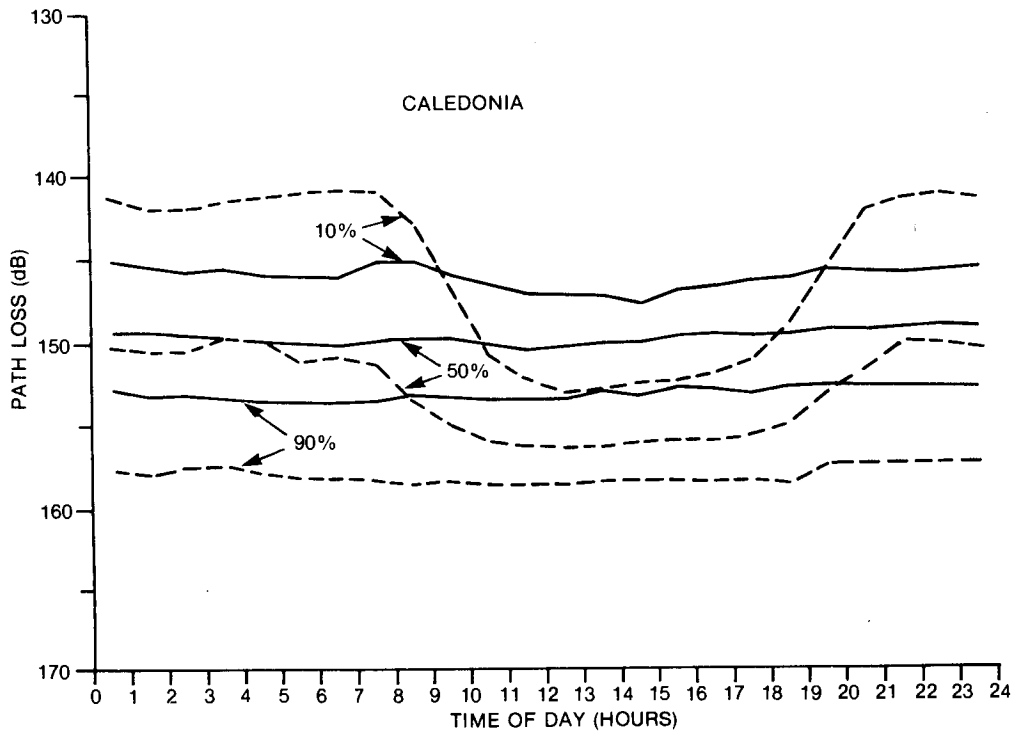


Figure 24. Diurnal variation of path loss for Caledonia. The solid lines are for winter (December–February), and the broken lines are for summer (June–August). Data from both years have been combined.

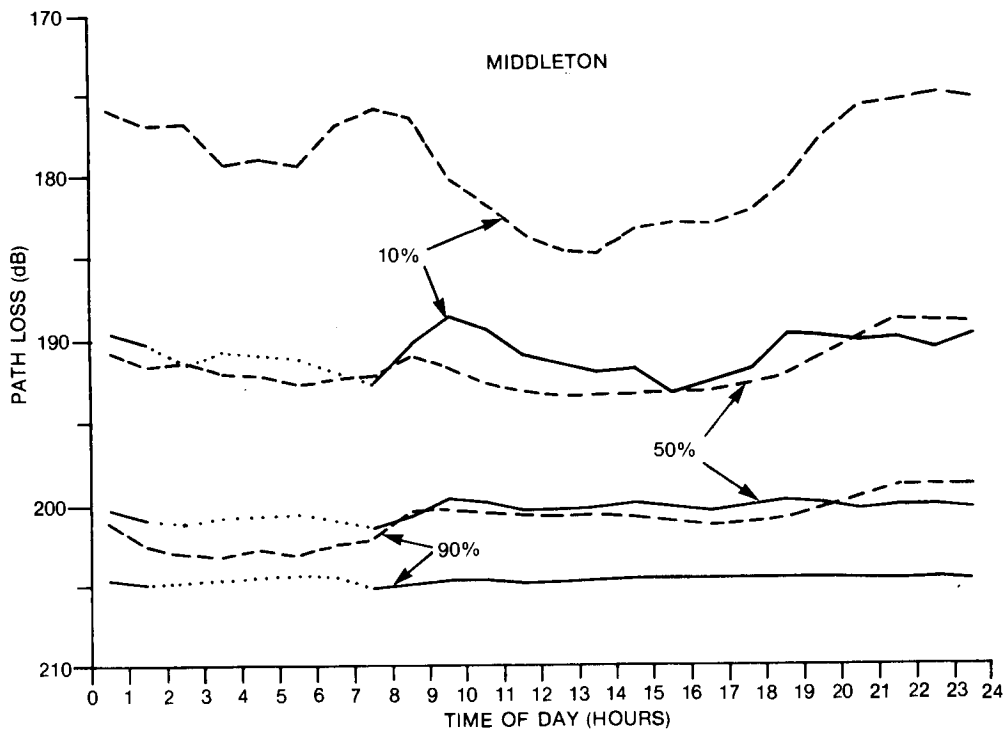


Figure 25. Diurnal variation of path loss for Middleton. The solid lines are for winter (December–February), and the broken lines are for summer (June–August). Data from both years have been combined. Dotted lines indicate interpolated data (see section 3.5).

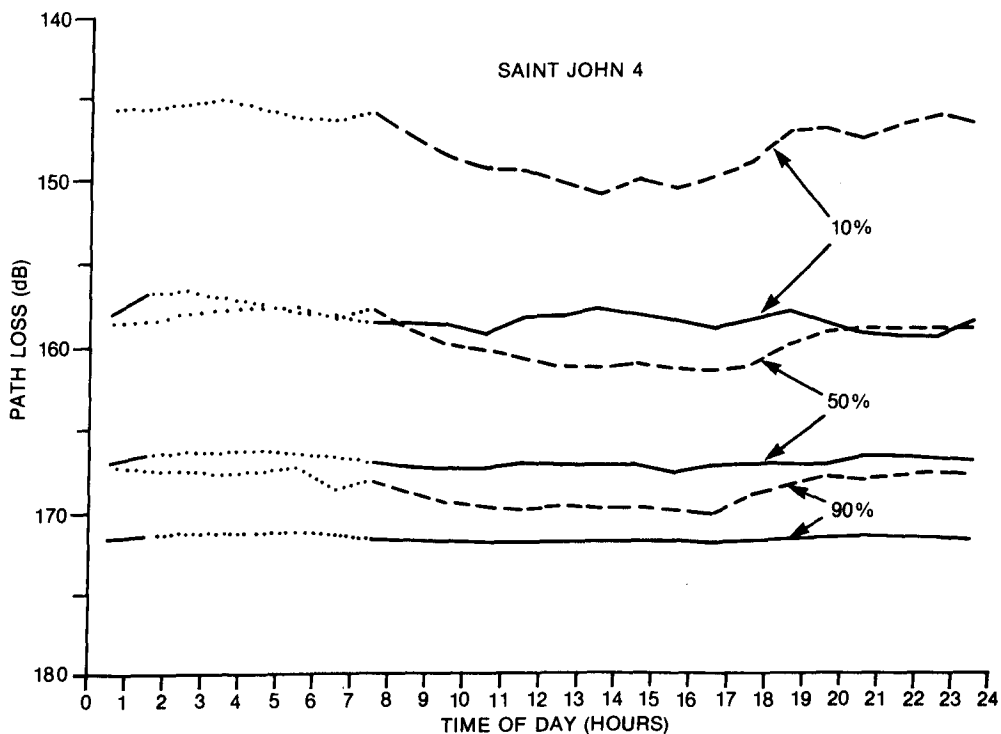


Figure 26. Diurnal variation of path loss for Saint John (channel 4). The solid lines are for winter (December-February), and the broken lines are for summer (June-August). Data from both years have been combined. Dotted lines indicate interpolated data (see section 3.5).

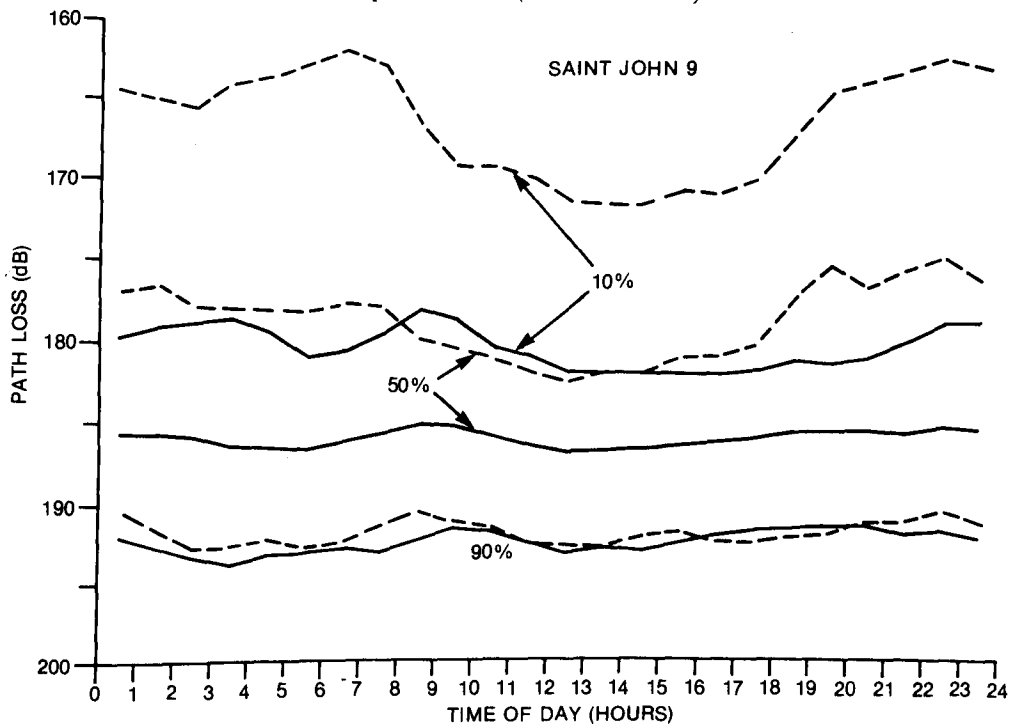


Figure 27. Diurnal variation of path loss for Saint John (channel 9). The solid lines are for winter (December-February), and the broken lines are for summer (June-August). Data from both years have been combined.

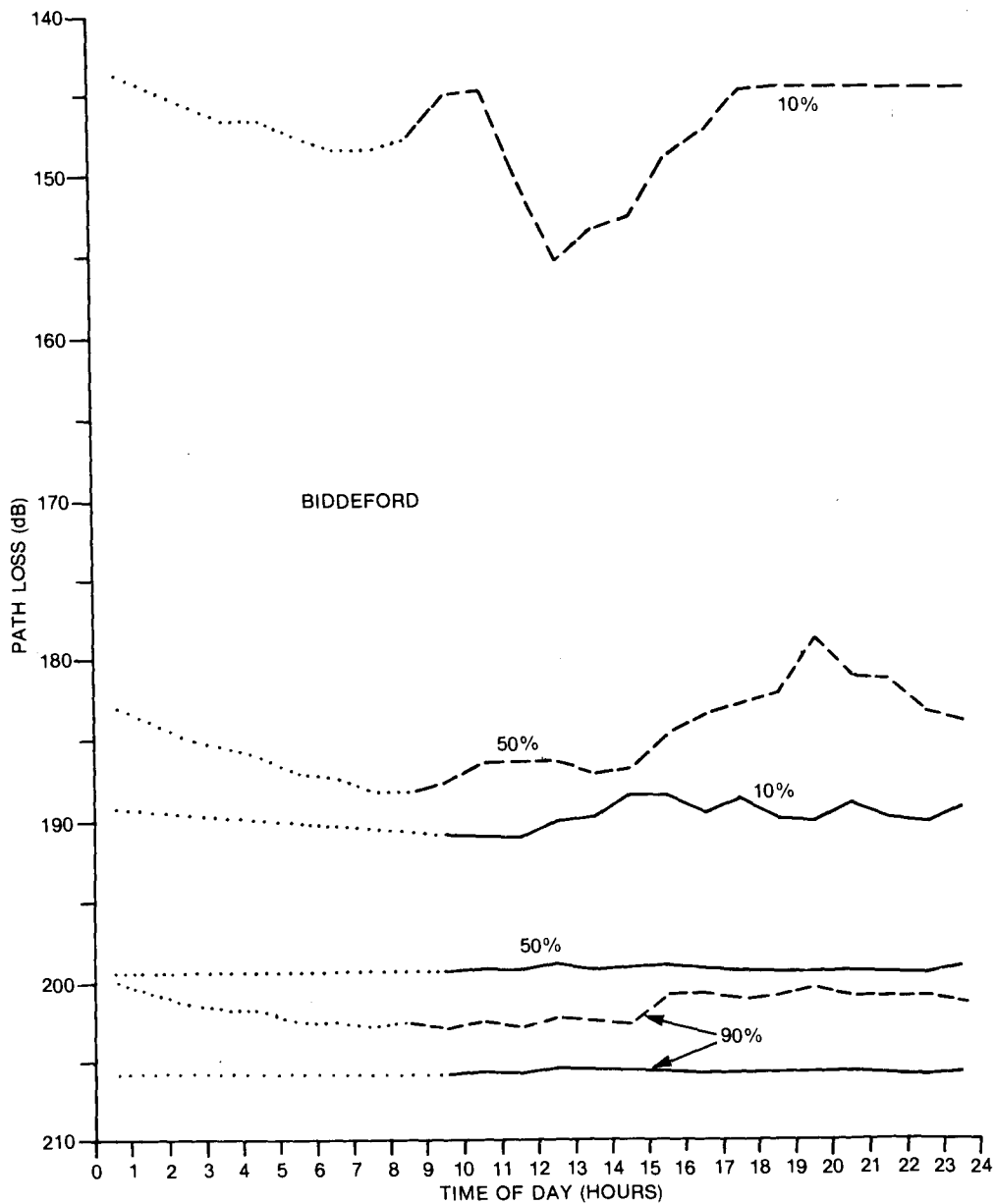


Figure 28. Diurnal variation of path loss for Biddeford. The solid lines are for winter (December-February), and the broken lines are for summer (June-August). Data from both years have been combined. Dotted lines indicate interpolated data (see section 3.5). The 10% summer curve is affected by receiver saturation.

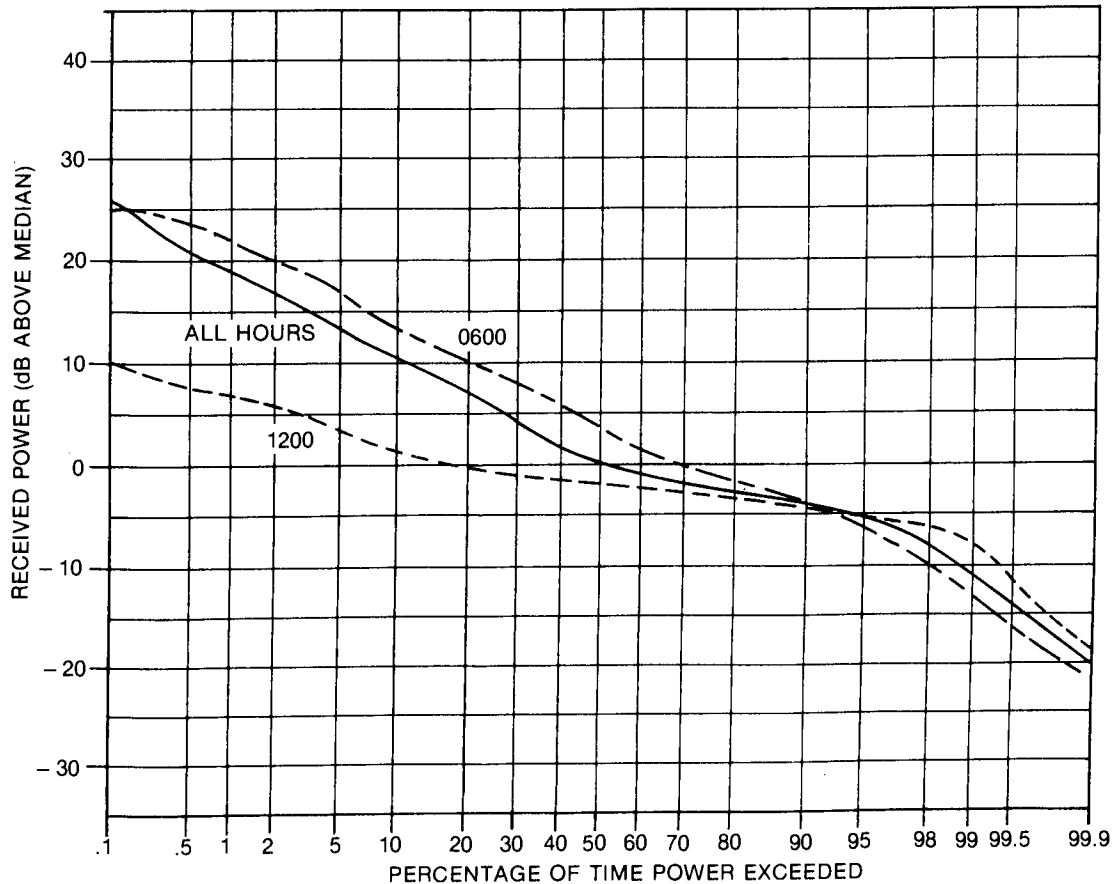


Figure 29. The distribution of received power for the Caledonia path in summer. The three curves represent the distributions for all hours, for the interval 0500 to 0700, and for the interval 1100 to 1300. Refer to Figure 24 for the diurnal variation at 10%, 50%, and 90%.

8.1.2 Numerical Summary of Diurnal Variation

To reduce the data on diurnal variations to a reasonable number of parameters, some curve fitting is required. For analytical convenience, diurnal variations are represented as sine waves, even though the observed changes between high and low signal levels are typically more abrupt than that. For any particular month of the year, then, the path loss L_d at hour t_h is assumed to be

$$L_d = \bar{L}_d + D \cos[(t_h - \hat{t}_h)\pi/12] \quad (9)$$

where, for that month, \bar{L}_d is the diurnal mean, D is the amplitude of diurnal variation, and \hat{t}_h is the hour of maximum path loss.

Equation 9 was fitted to the diurnal variation for each month. The mean values \bar{L}_d were not found to differ significantly from the monthly percentiles: most of the annual mean differences amounted to less than 0.5 dB. Therefore \bar{L}_d is not tabulated. For the 90% level, the diurnal variation is small, and only its annual mean amplitude is given. For the other percentiles, the diurnal phase \hat{t}_h does not vary much during the year; its annual mean values are given in Table 7.

However, the amplitude D does vary significantly, and its variation may be represented by an equation analogous to equation 4:

$$D = \bar{D} + B \cos[(t_d - \hat{r}_d)/58] \quad (10)$$

where \bar{D} , B and \hat{r}_d are constants, displayed in Table 7.

TABLE 7
Diurnal Variation

	Mean Amplitude			Annual Variation of Amplitude				Mean Phase	
	\bar{D}	\bar{D}	\bar{D}	B	\hat{r}_d	B	\hat{r}_d	\hat{t}_h	\hat{t}_h
	90%	50%	10%	50%	50%	10%	10%	50%	10%
	(dB)	(dB)	(dB)	(dB)	(days)	(dB)	(days)	(hours)	
Cal	0.6	1.8	3.9	1.6	14	3.2	16	13.5	14.2
Mid	0.8	1.1	3.3	0.5	15	1.1	29	10.1	14.5
St4	0.8	1.2	2.4	0.8	-3	1.2	24	15.1	14.9
St9	0.9	1.8	4.3	1.6	27	1.2	11	12.8	14.5
Bid	0.6	2.2	5.6	1.5	6	3.2	-80*	9.6	9.7

* The 10% curve is distorted by receiver saturation in summer; a phase of 8 days (the 50% value) may be more nearly correct.

8.2 MODEL OF DIURNAL VARIATION

8.2.1 Time Factor — Overland and Mixed Paths

From Table 7, we see that the diurnal phase constant for overland and mixed paths is about 14 hours. A diurnal cyclic factor may then be defined as:

$$c_d(t_h) = \cos[(t_h - 14)\pi/12] \quad (11)$$

Table 7 also shows that the phase \hat{r}_d of the annual variation of diurnal amplitude is about the same as the phase \hat{t}_d of the annual variation. Therefore the same cyclic factor $c_a(m)$ will be used.

8.2.2 Distance Factor — Overland and Mixed Paths

According to Rice et al.(1, section III 7.1), the range of the diurnal variation reaches a maximum just beyond the horizon, at least for continental temperate climates. Similarly, in the results reported here, the greatest diurnal variation occurs on the shortest path. A distance factor that fits the summer-time diurnal amplitudes fairly well is

$$f_2(d_e) = (d_e/100)^3 \exp[3(1 - d_e/100)] \quad (12)$$

This function is illustrated in Figure 30, along with the data.

8.2.3 Model of Diurnal Variation — Overland and Mixed Paths

For overland or mixed paths, the path loss for month m at hour t_h may be approximated as:

$$\begin{aligned} L_2(t_h, m, 10) &= L_1(m, 10) + f_2(d_e) [4 - 3.0c_a(m)]c_d(t_h) \\ L_2(t_h, m, 50) &= L_1(m, 50) + f_2(d_e) [2 - 1.5c_a(m)]c_d(t_h) \\ L_2(t_h, m, 90) &= L_1(m, 90) + f_2(d_e) [1 - 0.5c_a(m)]c_d(t_h) \end{aligned} \quad (13)$$

As mentioned in section 8.1.2, the diurnal mean was not found to be significantly different from the percentile for the month.

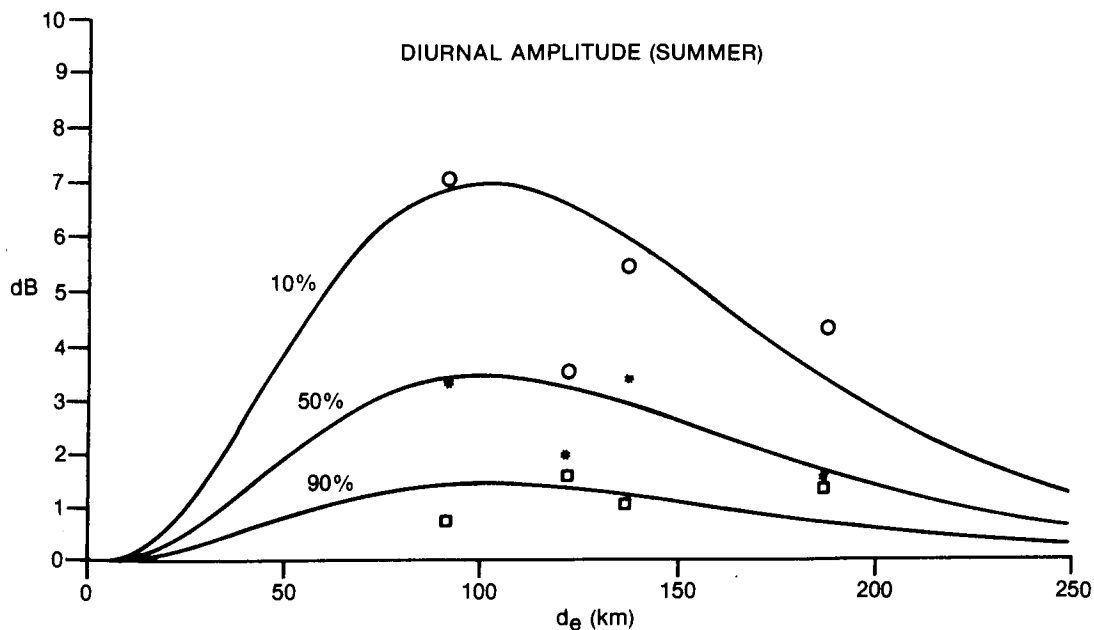


Figure 30. The annual maximum amplitude of the diurnal variation of received power as a function of effective distance, for overland and mixed paths. The points are obtained from Table 7. The percentiles 10, 50, 90 are represented by circles, asterisks, squares, respectively. The curves represent the function f_2 (equation 12) multiplied by 7, 3.5, and 1 dB.

8.2.4 Model of Diurnal Variation — Oversea Paths

For oversea paths, we have only the data from one path and the results from Sable Island (9). At VHF, the Sable Island results show no diurnal variation. At UHF, both Sable Island and Biddeford show diurnal variations during the summer only. Unfortunately, the phases do not agree. Furthermore, within each data set there seems to be a lack of consistency from month to month. The main variation seems to be random rather than diurnal. The best course may be to ignore the diurnal variation on oversea paths, at least until more data become available.

8.2.5 Other Measurements

There does not seem to be much information in the literature concerning diurnal variation. It is generally agreed that the greatest signal levels occur in the morning and the smallest occur in the afternoon. The diurnal range of hourly medians on the shortest Hebron path was found to be about 7 dB in summer. For comparison, Rice et al. (reference 1, Figure III.32) suggest 4 dB between six-hour averages, Boithias (3) suggests up to 15 dB, Boithias and Battesti (4) suggest up to 10 dB in temperate climates, and Palmer (reference 7, Table 7.1) suggests 5 to 10 dB.

9. CONCLUSIONS

The long-term median path losses predicted by standard methods agree with the measured values to within 10 dB if foliage attenuation is taken into account.

The distribution of received power levels for overland or mixed paths in the Atlantic region of Canada agrees with the curves published by NBS. For oversea paths, there is similar agreement for VHF, and for UHF for large percentages of time, but at UHF, the received power levels for small percentages of time exceed the published levels by 10 dB or more.

The annual variation is summarized by equation 7 for overland and mixed paths, and by equation 8 for oversea paths. The diurnal variation is summarized by equation 13 for overland and mixed paths, and is not modelled for oversea paths because of uncertainty about its behaviour. In all cases, the dependence on transmission path length is tentative.

10. ACKNOWLEDGEMENTS

The initial survey of potential receiving sites was made by J.R.R. Charron of CRC and W. Chang and G. Dodsworth of Technical University of Nova Scotia. Site selection was made by F.H. Palmer, who was initially responsible for the contract at CRC. C.P. Tou was the principal investigator at Technical University of Nova Scotia. The Maritime Telegraph and Telephone Company set up the receiving equipment on their site, in cooperation with C.P. Tou and B. Chang. D. Kaye of MT&T took care of the equipment on site and sent tape cartridges to CRC. J.R.R. Charron and G.N. Reed of CRC were responsible for the receivers and data logger respectively, modifying and maintaining them as necessary. J.R.R. Charron accompanied the author on a field trip after the monitoring period to measure field strengths.

11. REFERENCES

1. Rice, P. L., A. G. Longley, K. A. Norton, and A. P. Barsis, Transmission Loss Predictions for Tropospheric Communication Circuits, *National Bureau of Standards Technical Note 101, revised, Vols. I and II*, AD 687820 and AD687821, NTIS, Springfield, Va., USA, 1967.
2. Hall, M. P. M., *Effects of the Troposphere on Radio Communication*, IEE Electromagnetic Wave Series 8, Peter Peregrinus Ltd., London, 1979.
3. Boithias, L., *Propagation des Ondes Radioélectriques dans l'Environnement Terrestre*, Dunod, Paris, 1983.
4. Boithias, L. and J. Battesti, Propagation due to Tropospheric Inhomogeneities, *IEE Proceedings, Vol. 130, Part F*, 657-664, 1983.
5. Propagation Data Required for Trans-Horizon Radio-Relay Systems, Report 238-4, *Recommendations and Reports of the CCIR, Vol. V*, ITU, Geneva, 1982.
6. The Evaluation of Propagation Factors in Interference Problems between Stations on the Surface of the Earth at Frequencies above about 0.5 GHz, Report 569-2, *Recommendations and Reports of the CCIR, Vol. V*, ITU, Geneva, 1982.
7. Palmer, F. H., Report on the Great Lakes Propagation Measurement Program: Comparisons of the Canadian Data with the Predictions of FCC R-6602, *CRC Report No. 1332*, Dept. of Communications, Ottawa, 1980.
8. Tou, C. P., The Propagation Measurements of VHF/UHF Signals Received over Long East Coast Paths of Canada, Report to Dept. of Communications, Technical University of Nova Scotia, Halifax, 1983.
9. Lonc, W. P., VHF/UHF Signal Statistics as Functions of Polarization and Frequency over a Long Salt-Water Path, Report to Dept. of Communications, St. Mary's University, Halifax, 1984.
10. Palmer, F. H., The Communications Research Centre VHF/UHF Propagation Prediction Program: An Overview, *Can. Elec. Eng. J.*, Vol. 6, No. 4, 3-9, 1981.
11. Whitteker, J. H., The CRC Topographic Data Base, *CRC Report No. 1353*, Dept. of Communications, Ottawa, 1982.
12. *Atlas of Ground-Wave Propagation Curves for Frequencies between 30 Mc/s and 300 Mc/s*, ITU, Geneva, 1955.
13. Rice, P. L., Some Effects of Buildings and Vegetation on VHF/UHF Propagation, *1971 IEEE Mountain-West EMC Conference Record*, 1-10, 1971.
14. Television Broadcasting Transmitters Operating in the 54-88 MHz, 174-216 MHz and 470-806 MHz Frequency Bands, *Dept. of Communications Radio Standards Specification RSS-154 (Issue 2, revised)*, 1984.

APPENDIX A

Mean Carrier Amplitude

A narrow-band receiver tuned to the carrier frequency of an amplitude-modulated signal responds to the mean (time-average) amplitude. In effect, the frequency filter does a Fourier analysis of the incoming signal, and accepts only the Fourier component at the carrier frequency. The Fourier component at the carrier frequency is the mean carrier amplitude.

A television transmitter emits its maximum authorized power only during the synchronizing pulses (Reference 14, definition 6.1.1). During the picture scan, the video carrier is modulated, as illustrated in Figure A1. The modulation follows a standard pattern between horizontal picture lines (illustrated), and for the twenty-one lines between frames (not illustrated). During picture transmission, the carrier amplitude must vary between two specified levels, labelled 0 and 100 IRE units.

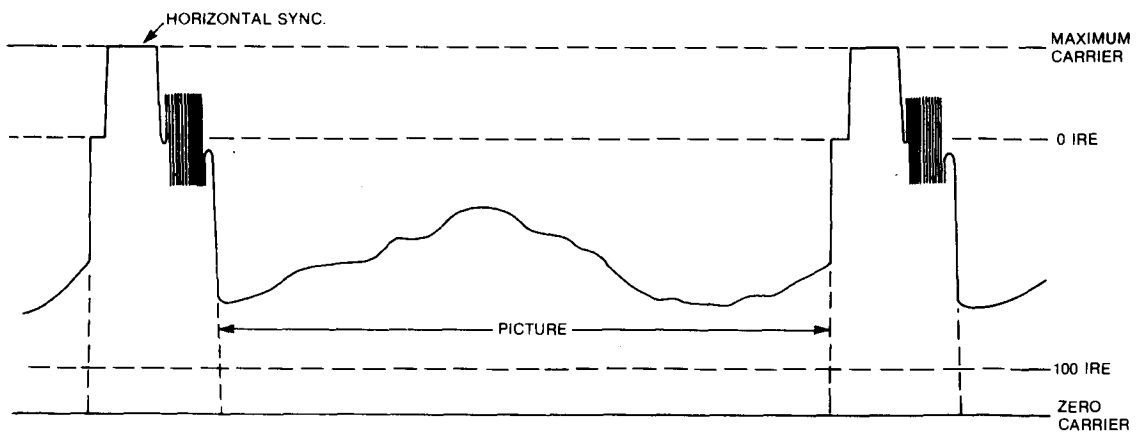


Figure A1. Video carrier amplitude during a horizontal scan, from Reference 14. With respect to the maximum carrier amplitude, the IRE scale is defined to be zero at 0.75 and one hundred at 0.125.

In order to estimate typical carrier levels during picture transmission, the signals from the five Ottawa television stations were displayed, in turn, on a video waveform monitor. The average video amplitude was estimated and recorded in each case. This procedure continued for about two hours, with 52 samples, in order to survey a variety of program material. The extreme and average results are shown in Table A1.

TABLE A1
Examples of Video Signal Levels

Picture	IRE Units	Mean Signal (dB below maximum)
black	7.5	2.7
disco scene	15	3.1
average	42	4.9
cartoon	65	6.7
white	100	10.6

The average carrier amplitude was found in the following way: The carrier amplitude A_p during picture transmission was found from

$$A_p = 0.75 - \text{IRE}/160 \quad (A1)$$

where IRE is the carrier level in IRE units. Equation A1 follows directly from the definition of IRE units. The mean carrier amplitude A_c was found from

$$A_c = 0.20 + 0.754 A_p \quad (A2)$$

The coefficients of equation A2 were found graphically.

The average carrier amplitude estimated here is probably in error by less than 1 dB. Such an error will not contribute significantly to the error in estimating long-term path loss. The possibility remains that the statistics of variation are contaminated by hour-to-hour changes in program material. However, the effect of these changes is expected to be small. The extremes of observed picture level (a disco scene, a particular cartoon), differ from the mean by only 2 dB. Most variations are smaller than this, and not strongly correlated with season or hour of day.

APPENDIX B

Post-mortem measurements of field strength

In September 1984, field strengths were measured close to the Middleton and Saint John transmitters in order to verify that their ERP's were as had been assumed. Measurements were also made on a peninsula called Digby Neck, about 128 km from the Saint John transmitter, across the Bay of Fundy. In all cases, the measurements were made close to the great-circle path between the transmitter and Hebron. The receiving antennas were Yagis, mounted on a 3-metre mast. The measurements at Middleton and Saint John were all made at sites from which the transmitting tower was clearly visible. The results of these measurements are given in Table B1.

TABLE B1
Results of ERP Measurements

Location	Distance from Tx (km)	Path Loss in Excess of Free Space (dB)	
		Saint John Channel 4	Channel 9
Westfield Golf Course	15.4	0	8
Ingleside Heights	16.8	-3	1
		Middleton Channel 8	
Vegetable Farm	8.5	5	
Campbell Meadows	10.3	9	
Hill above Torbrook Mines	20.0	8	
Highway #10	27.5	6	

Of the two receiving sites at Saint John, the one at Ingleside Heights was close to ideal, with the terrain descending steeply in the direction of the transmitter, and with no obstructions. At the golf-course site, the terrain descended less steeply, and some foliage may have intruded into the first Fresnel zone. Foliage absorption increases with frequency. The results support the conclusion that the ERP of both channels was as assumed.

Of the receiving sites at Middleton, none was quite as good as the better one at Saint John. The best ones were the vegetable farm and Highway #10. The vegetable farm was completely clear of obstructions, but the flat farmland may have supported reflections. The Highway #10 site overlooked descending terrain, but it is possible that some distant foliage affected the result. The results suggest that the ERP in the direction of Hebron may be a few dB lower than assumed, but the evidence is not conclusive, and no change was made in the analysis.

The results of the Digby-Neck measurements are shown in Figure B1, along with the curves obtained from spherical diffraction calculations. The best receiving site was at Sandy Cove, where the antenna overlooked the sea from the top of a high cliff. From the other sites, the receiving antenna also had a clear view of the sea, except that at Culloden there were trees below the line of sight between the antenna and the ocean. Considering that at 128 km from the transmitter, some time variations due to atmospheric effects can be expected, the results indicate that the calculation gives the correct result over the Bay of Fundy.

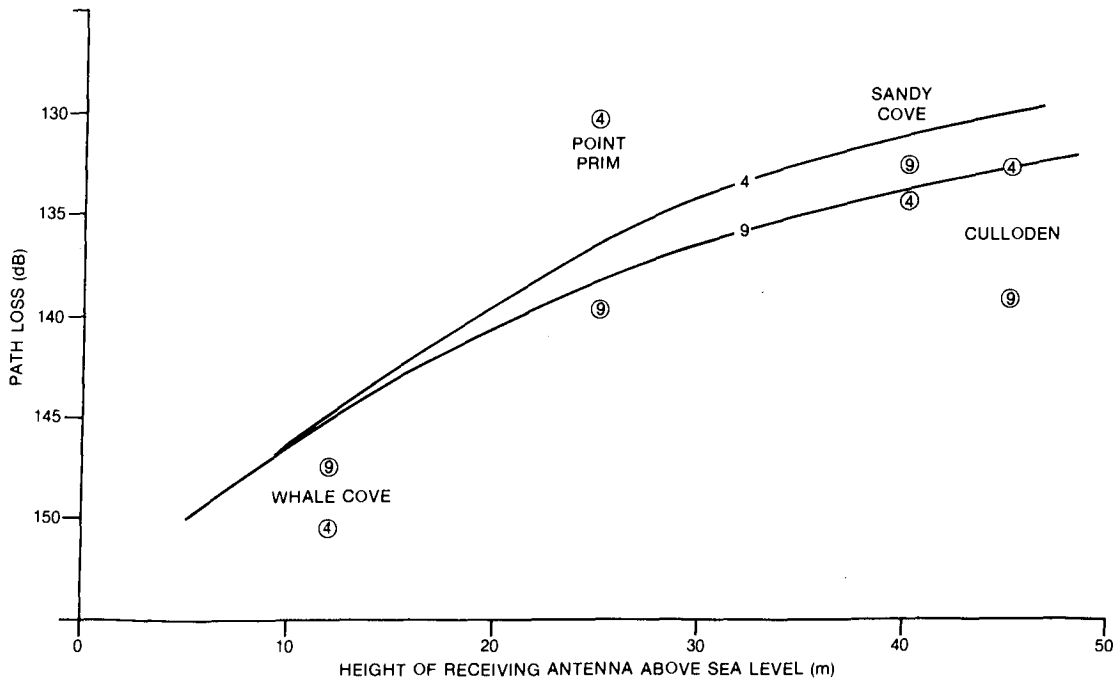


Figure B1. Path loss across the Bay of Fundy from Saint John to Digby Neck on September 11 and 12, 1984. The encircled numerals (channel numbers) indicate measured losses, while the curves show the results of spherical diffraction calculations.

TK
5102.5
C673e
#1380


DATE DUE
DATE DE RETOUR

NOV 9 1985			
DEC 1 1985			
DEC 10 1985			
FEB 2 1986			

LOWE-MARTIN No. 1137

CRC LIBRARY/BIBLIOTHEQUE CRC
TK5102.5 C673e #1380 c. b
Whittaker, J. H.

INDUSTRY CANADA / INDUSTRIE CANADA



209005

